Optical Bragg accelerators

Amit Mizrahi and Levi Schächter
Department of Electrical Engineering, Technion-IIT, Haifa 32000, Israel
(Received 4 November 2003; revised manuscript received 26 January 2004; published 23 July 2004)

It is demonstrated that a Bragg waveguide consisting of a series of dielectric layers may form an excellent optical acceleration structure. Confinement of the accelerating fields is achieved, for both planar and cylindrical configurations by adjusting the first dielectric layer width. A typical structure made of silica and zirconia may support gradients of the order of 1 GV/m with an interaction impedance of a few hundreds of ohms and with an energy velocity of less than 0.5c. An interaction impedance of about 1000 Ω may be obtained by replacing the Zirconia with a (fictitious) material of $\varepsilon=25$. Special attention is paid to the wake field developing in such a structure. In the case of a relatively small number of layers, it is shown that the total electromagnetic power emitted is proportional to the square of the number of electrons in the macrobunch and inversely proportional to the number of microbunches; this power is also inversely proportional to the square of the internal radius of the structure for a cylindrical structure, and to the width of the vacuum core in a planar structure. Quantitative results are given for a higher number of dielectric layers, showing that in comparison to a structure bounded by metallic walls, the emitted power is significantly smaller due to propagation bands allowing electromagnetic energy to escape.

DOI: 10.1103/PhysRevE.70.016505 PACS number(s): 41.75.Lx, 41.20.Jb, 41.60.Bq, 42.81.Qb

I. INTRODUCTION

Indications that solid-state lasers will reach wall-plug to light efficiencies of 30% or more, make a laser-driven vacuum-accelerator increasingly appealing. Since at the wavelength of relevant lasers, dielectrics may sustain a significantly higher electric field and transmit power with reduced loss comparing to metals, the basic assumption is that laser acceleration structures will be made of dielectrics. Closed optical structures and near-field accelerators with dimensions comparable to the wavelength are both being considered. Examples of these two are (a) the LEAP [1] crossed laser beam accelerator where the interaction between the crossed laser beams and the particles is limited by slits to satisfy the Lawson-Woodward theorem [2,3] and (b) the two-dimensional *photonic band-gap* (PBG) concept where a laser pulse is guided in a vacuum tunnel bored in the center of a two-dimensional transverse periodic structure [4].

Motivated by the low-loss of Bragg dielectric *planar* mirrors used in high-power lasers, it is suggested that this concept be harnessed in order to confine the laser-field in an optical one-dimensional PBG acceleration structure. Its essence is to form a hollow optical waveguide, either planar or cylindrical, consisting of an almost perfect reflector comprised out of an array of dielectric layers. Lithography, which would result in planar structures, and optical fiber drawing are manufacturing techniques that seem well suited for such laser driven structures that have typical dimensions of a few microns.

The theory of Bragg reflection waveguides was developed by Yeh *et al.* [5,6], and recently there has been a growing interest in using such cylindrical structures as low-loss optical fibers in long distance communications. Asymptotic analysis of these so called "*hollow Bragg fibers*" shows that for large radii the cylindrical structure is strongly analogous to a planar structure [7,8]. Investigation of the propagating modes was also performed [9,10], and fabrication of Bragg fibers was demonstrated [11,12]. In the aforementioned papers the configuration considered is of a vacuum tunnel bordering a Bragg mirror, i.e., quarter-wavelength alternating dielectric layers. Hence, the resulting propagation modes resemble those of a hollow metallic waveguide. A basic requirement for an acceleration structure is that it will support the propagation of a mode with longitudinal wave number ($k_z=\omega/c$), which will accelerate ultrarelativistic particles. It is one of the purposes of this study to adapt the design procedure so that this unique mode is confined for a given laser wavelength λ_0.

Further insight into the nature of such future acceleration structures is gained by analysis of the electromagnetic wake field generated by a macrobunch traversing the device. The wake field, as a side effect of having charged particles in high velocity motion, may cause undesirable results. A significant effort has been directed in recent years to the analysis of wakes generated by electron bunches in the vicinity of dielectric structures. However, these studies focus on dielectric-loaded structures with *metallic* boundaries such as the partially dielectric loaded planar transmission line [13,14], the partially dielectric loaded rectangular waveguide [15,16] and the partially dielectric loaded cylindrical waveguide [17,18] (and more recently Ref. [19]), which are illustrated in Fig. 1. Pure dielectric structures were investigated in Ref. [20], where a vacuum tunnel inside a homogeneous dielectric material was considered, and in Ref. [21] a general method for treating cylindrical structures with a vacuum tunnel and arbitrary surrounding geometry was presented.

The organization of the paper is as follows. The first part of this paper treats the *homogeneous* solutions of the wave equation within the Bragg reflection waveguide, required for ensuring adequate propagation of the accelerating electromagnetic wave injected from an external source. In Sec. II the acceleration structures are described in detail, and the homogeneous electromagnetic problem is formulated under

 ©2004 The American Physical Society

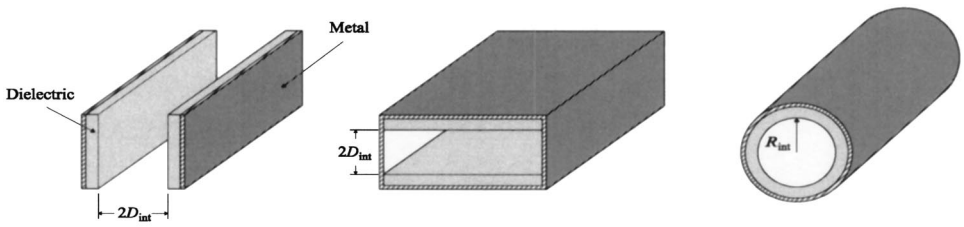

FIG. 1. Typical closed structure configurations considered in the literature. Left: Partially dielectric loaded planar transmission line. Middle: Partially dielectric loaded rectangular waveguide. Right: Partially dielectric loaded cylindrical waveguide.

the constraint of longitudinal wave number $k_z=\omega/c$; this section provides us with basic *analysis* tools of such a structure. Relying on this formulation. we develop in Sec. III *design* criteria of the structure, so that the required etectromagnetic field is confined, and characteristics of the confinement are discussed. In Sec. IV an analysis of the behavior of the proposed structures as accelerators is presented in terms of the accelerator parameters (interaction impedance, group velocity, and maximum electric field), and some tradeoffs are discussed. In addition to the general analysis, a specific example of a typical structure made out of silica ($\varepsilon=2.1$) and zirconia ($\varepsilon=4$) is given. The second part of this study deals with *nonhomogeneous* solutions of the wave equations corresponding to the wake field generated by charges traversing the device. In Sec. V the wake field generated by a single bunch as well as a train of microbunches is examined for both the planar and cylindrical cases. For the case of a line charge in a planar structure, formulation is provided, and additional insight is gained by comparing the result of the Bragg structure with those of the dielectric loaded planar metallic or perfect magnetic conductor transmission lines. A qualitative approach is given for the estimation of the emitted power in the case of a weak mirror, i.e., a small number of Bragg layers, and quantitative results are given for different numbers of Bragg layers.

II. DESCRIPTION OF THE SYSTEM

As indicated in the introduction, two types of devices are investigated in this work, one is a planar and the other is a cylindrical dielectric waveguide. Both devices consist of dielectric layers surrounding a vacuum region. The planar structure is symmetric relative to the central plane, and the cylindrical structure is azimuthally symmetric. A detailed description of each device is given next, the electromagnetic field in each region is formulated, and the relations between the field components in the different layers are established using a matrix formulation.

A. Planar structure

Consider a planar symmetric dielectric waveguide ($\partial/\partial y=0$), as illustrated in Fig. 2, which will be referred to as the planar Bragg accelerator (PBA). The PBA has a vacuum inner region of width $2D_{\mathrm{int}}$ and surrounding alternating periodic layers. The interfaces between the dielectrics are at constant x planes, and they extend to infinity in z and y directions. The layers are made of two lossless materials ε^{I} and $\varepsilon^{\mathrm{II}}$, the first layer having a relative dielectric coefficient ε^{I}. The vacuum region is labeled $\nu=0$, and the outermost region extends to infinity in x and is labeled $\nu=N+1$. In the framework of this notation the thickness of each dielectric layer is denoted by Δ_ν, whereas the dielectric coefficient is denoted by ε_ν. The distance from the center of the structure to the middle of the νth layer is denoted by D_ν. Assuming a steady-state regime ($e^{j\omega t}$) we focus on the mode having a phase velocity equal to the speed of light, or explicitly in the vacuum region the required electromagnetic field reads

$$E_z = E_0 e^{-j(\omega/c)z},$$

$$E_x = j\frac{\omega}{c} x E_0 e^{-j(\omega/c)z},$$

$$H_y = \frac{j}{\eta_0}\frac{\omega}{c} x E_0 e^{-j(\omega/c)z}. \tag{1}$$

In a specific dielectric layer ν, a wave propagating with phase velocity c has the following field components:

$$E_z = (A_\nu e^{-jk_\nu x} + B_\nu e^{+jk_\nu x}) e^{-j(\omega/c)z},$$

$$E_x = \frac{-1}{\sqrt{\varepsilon_\nu - 1}}(A_\nu e^{-jk_\nu x} - B_\nu e^{+jk_\nu x}) e^{-j(\omega/c)z},$$

$$H_y = \frac{-1}{Z_\nu}(A_\nu e^{-jk_\nu x} - B_\nu e^{+jk_\nu x}) e^{-j(\omega/c)z}, \tag{2}$$

wherein

$$Z_\nu \triangleq \eta_0 \sqrt{\varepsilon_\nu - 1}/\varepsilon_\nu \tag{3}$$

is the transverse wave impedance and $\eta_0 \approx 377\Omega$ is the vacuum impedance. Note that as a function of ε_ν this impedance has a maximum for $\varepsilon_\nu=2$, a fact which as we shall see subsequently, is of great significance. Finally,

$$k_\nu \triangleq \frac{\omega}{c}\sqrt{\varepsilon_\nu - 1} \tag{4}$$

is the transverse wave number.

In order to establish the relation between the amplitudes of the various layers, we next define $\chi_\nu^{(\pm)} \triangleq k_\nu(D_\nu \pm \Delta_\nu/2)$ and impose the continuity of E_z and H_y at each interface between layer $\nu(\neq 0)$ and layer $\nu+1$; the resulting equations are

$$A_\nu e^{-j\chi_\nu^{(+)}} + B_\nu e^{+j\chi_\nu^{(+)}} = A_{\nu+1} e^{-j\chi_{\nu+1}^{(-)}} + B_{\nu+1} e^{+j\chi_{\nu+1}^{(-)}}, \tag{5}$$

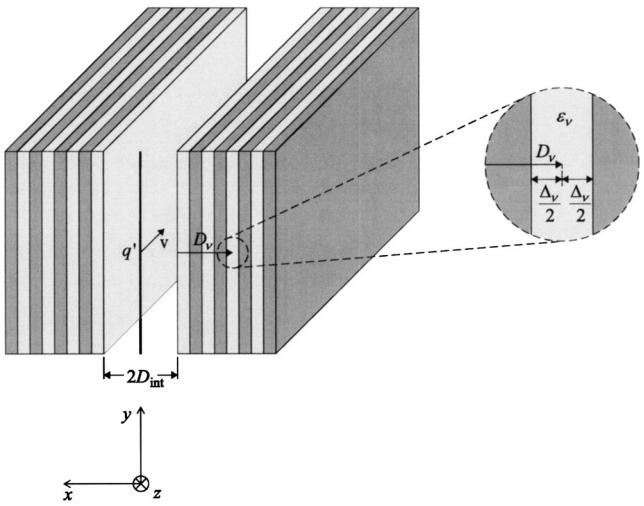

FIG. 2. Schematic drawing of the planar Bragg accelerator (PBA).

$$\frac{1}{Z_\nu}(A_\nu e^{-j\chi_\nu^{(+)}} - B_\nu e^{+j\chi_\nu^{(+)}}) = \frac{1}{Z_{\nu+1}}(A_{\nu+1}e^{-j\chi_{\nu+1}^{(-)}} - B_{\nu+1}e^{+j\chi_{\nu+1}^{(-)}}) \tag{6}$$

Further defining the matrices

$$\mathcal{D}_\nu^{(\pm)} \triangleq \begin{pmatrix} e^{-j\chi_\nu^{(\pm)}} & e^{+j\chi_\nu^{(\pm)}} \\ \frac{\eta_0}{Z_\nu}e^{-j\chi_\nu^{(\pm)}} & -\frac{\eta_0}{Z_\nu}e^{+j\chi_\nu^{(\pm)}} \end{pmatrix}, \tag{7}$$

Eqs. (5) and (6) can be expressed as

$$\mathcal{D}_\nu^{(+)}\begin{pmatrix} A_\nu \\ B_\nu \end{pmatrix} = \mathcal{D}_{\nu+1}^{(-)}\begin{pmatrix} A_{\nu+1} \\ B_{\nu+1} \end{pmatrix}. \tag{8}$$

Consequently, it is now possible to write the amplitudes in layer $\nu+1$ in terms of the amplitudes in layer ν

$$\begin{pmatrix} A_{\nu+1} \\ B_{\nu+1} \end{pmatrix} = [\mathcal{D}_{\nu+1}^{(-)}]^{-1}\mathcal{D}_\nu^{(+)}\begin{pmatrix} A_\nu \\ B_\nu \end{pmatrix} \equiv \mathcal{T}^{\nu+1,\nu}\begin{pmatrix} A_\nu \\ B_\nu \end{pmatrix}; \tag{9}$$

$\mathcal{T}^{\nu+1,\nu}$ being the *transition matrix* from layer ν to layer $\nu+1$. For the transition from the vacuum region $\nu=0$ to layer $\nu=1$, the continuity equation of E_z and H_y is

$$\begin{pmatrix} E_0 \\ -j\frac{\omega}{c}D_{\rm int}E_0 \end{pmatrix} = \mathcal{D}_1^{(-)}\begin{pmatrix} A_1 \\ B_1 \end{pmatrix}. \tag{10}$$

In the outermost layer $(N+1)$ there is no inward wave $(B_{N+1}=0)$, and the amplitudes are therefore

$$\begin{pmatrix} A_{N+1} \\ 0 \end{pmatrix} = \mathcal{T}^{N+1,N}\mathcal{T}^{N,N-1}\cdots\mathcal{T}^{3,2}\mathcal{T}^{2,1}[\mathcal{D}_1^{(-)}]^{-1}\begin{pmatrix} E_0 \\ -j\frac{\omega}{c}D_{\rm int}E_0 \end{pmatrix}. \tag{11}$$

Further defining

$$\Theta \triangleq \begin{pmatrix} \Theta_{11} & \Theta_{12} \\ \Theta_{21} & \Theta_{22} \end{pmatrix} = \{\mathcal{T}^{N+1,N}\mathcal{T}^{N,N-1}\cdots\mathcal{T}^{3,2}\mathcal{T}^{2,1}[\mathcal{D}_1^{(-)}]^{-1}\}^{-1}, \tag{12}$$

we find that for an eigenmode to exist, the following condition ought to be satisfied, rewriting Eq. (11) utilizing definition (12):

$$\begin{pmatrix} 1 & -\Theta_{11} \\ -j\frac{\omega}{c}D_{\rm int} & -\Theta_{21} \end{pmatrix}\begin{pmatrix} E_0 \\ A_{N+1} \end{pmatrix} = 0. \tag{13}$$

The determinant of the matrix is not zero, but as will be shown in what follows, it can be made arbitrarily small subject to a design procedure and according to the number of layers being used. Moreover, it can readily be shown that the ratio of the two amplitudes is

$$\frac{A_{N+1}}{E_0} = \frac{1}{\Theta_{11}} = -j\frac{\omega}{c}D_{\rm int}\frac{1}{\Theta_{21}}. \tag{14}$$

Next, we shall repeat this analysis for a cylindrically symmetric structure.

B. Cylindrical structure

The cylindrical Bragg accelerator (CBA) consists of a series of alternating concentric dielectric layers surrounding a vacuum region of radius $R_{\rm int}$, as depicted in Fig. 3. Each layer ν is of thickness Δ_ν and the average of its internal and external radii is R_ν; the dielectric coefficient of each layer is denoted by ε_ν similarly to the PBA. An analysis analogous to the one presented in the previous section is performed in cylindrical coordinates. In the vacuum core $(\nu=0)$ the required field components are

$$E_z = E_0 e^{-j(\omega/c)z},$$

$$E_r = \frac{j}{2}\frac{\omega}{c}rE_0 e^{-j(\omega/c)z},$$

$$H_\phi = \frac{j}{2\eta_0}\frac{\omega}{c}rE_0 e^{-j(\omega/c)z}. \tag{15}$$

It is now worth mentioning that these expressions for the transverse electric and magnetic fields include a factor of $1/2$ that does not appear in the PBA case (1), implying that for a given gradient on axis, and for the same aperture, the total electric field is larger at the vacuum-dielectric interface than in the PBA. This issue will be further discussed subsequently. In some layer ν, the field components read

$$E_z = [A_\nu H_0^{(2)}(k_\nu r) + B_\nu H_0^{(1)}(k_\nu r)]e^{-j(\omega/c)z},$$

$$E_r = \frac{j}{\sqrt{\varepsilon_\nu - 1}}[A_\nu H_1^{(2)}(k_\nu r) + B_\nu H_1^{(1)}(k_\nu r)]e^{-j(\omega/c)z},$$

$$H_\phi = \frac{j}{Z_\nu}[A_\nu H_1^{(2)}(k_\nu r) + B_\nu H_1^{(1)}(k_\nu r)]e^{-j(\omega/c)z}. \tag{16}$$

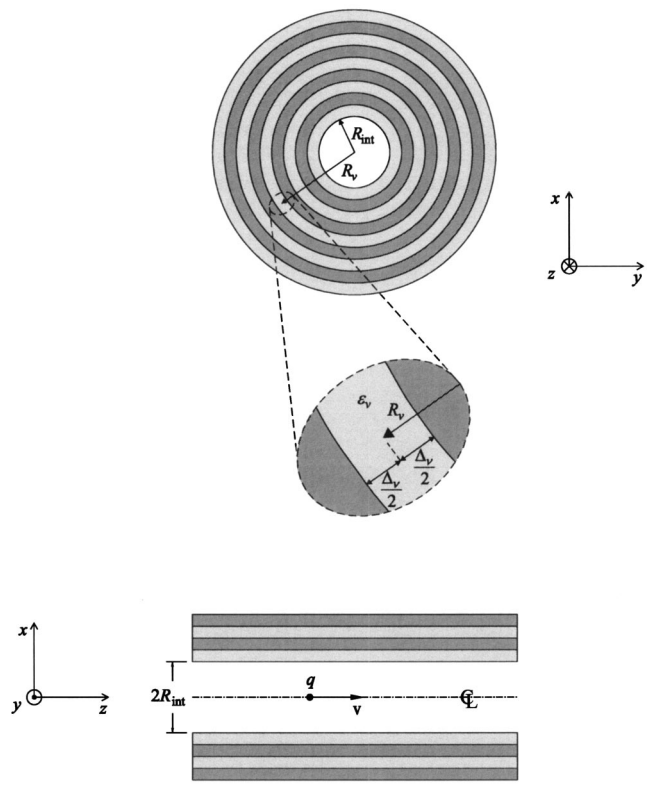

FIG. 3. Schematic drawing of the cylindrical Bragg accelerator (CBA).

Defining $\chi_\nu^{(\pm)} \triangleq k_\nu(R_\nu \pm \Delta_\nu/2)$, the matrices (7) take the form

$$\mathcal{D}_\nu^{(\pm)} \triangleq \begin{pmatrix} H_0^{(2)}(\chi_\nu^{(\pm)}) & H_0^{(1)}(\chi_\nu^{(\pm)}) \\ \frac{\eta_0}{Z_\nu} H_1^{(2)}(\chi_\nu^{(\pm)}) & \frac{\eta_0}{Z_\nu} H_1^{(1)}(\chi_\nu^{(\pm)}) \end{pmatrix}. \tag{17}$$

On the boundary of the vacuum core the continuity conditions are

$$\begin{pmatrix} E_0 \\ \frac{1}{2}\frac{\omega}{c} R_{\text{int}} E_0 \end{pmatrix} = \mathcal{D}_1^{(-)} \begin{pmatrix} A_1 \\ B_1 \end{pmatrix}, \tag{18}$$

and finally, the relation between the amplitude in the outermost layer to the amplitude in the vacuum core is given by

$$\frac{A_{N+1}}{E_0} = \frac{1}{\Theta_{11}} = \frac{1}{2}\frac{\omega}{c} R_{\text{int}} \frac{1}{\Theta_{21}}, \tag{19}$$

wherein the matrix Θ is defined similarly to Eq. (12).

III. FIELD CONFINEMENT

In order for the proposed structures to support the accelerating fields for a particular wavelength λ_0, transverse confinement is required. In Sec. II we have developed the necessary tools for the *analysis* of a multilayered structure. It is our purpose in this section to develop a *design* procedure that ensures the confinement of the required electromagnetic field at the specific wavelength λ_0. Its outcome will be a set of geometric parameters, namely, the thicknesses of the various dielectric layers, given the available dielectric coefficients of the materials. Here we extend an approach introduced by Yeh *et al.* both for the PBA [5] and for the CBA [6], so that the specific field distribution prescribed by Eqs. (1) and (15) are eigenmodes of the structure. Particularly, the significance of the role played by the width of the first layer is emphasized.

A. PBA design procedure

1. Infinite periodic structure analysis

With the aim of understanding the confinement process, we examine the propagation in the transverse direction in a planar structure. For now, we shall assume that the structure is *periodic and infinite* in both directions of *x*. The vacuum core and the first layer ($\nu=1$) will be taken into account in the following subsection. One period of the structure consists of two layers of widths Δ_2 and Δ_3, and dielectric coefficients ε_2 and ε_3 respectively, in consistency with the definitions of Sec. II.

The propagation in the periodic structure can be described by its transition matrix through one period. Transition through one unit cell of the periodic structure can be described by traversing one discontinuity from material 3 to material 2, propagating the width Δ_2, traversing a discontinuity from material 2 to material 3, and propagating the width Δ_3. Explicitly this is given by

$$T \triangleq \begin{pmatrix} T_{11} & T_{12} \\ T_{21} & T_{22} \end{pmatrix} = \begin{pmatrix} e^{-j\Psi_3} & 0 \\ 0 & e^{j\Psi_3} \end{pmatrix} \begin{pmatrix} \rho_2^{(+)} & -\rho_2^{(-)} \\ -\rho_2^{(-)} & \rho_2^{(+)} \end{pmatrix} \times \begin{pmatrix} e^{-j\Psi_2} & 0 \\ 0 & e^{j\Psi_2} \end{pmatrix} \begin{pmatrix} \rho_3^{(+)} & \rho_3^{(-)} \\ \rho_3^{(-)} & \rho_3^{(+)} \end{pmatrix}, \tag{20}$$

wherein $\Psi_\nu \triangleq k_\nu \Delta_\nu$, $\rho_\nu^{(\pm)} \triangleq (Z_3 \pm Z_2)/(2Z_\nu)$, and $\nu=2$ or 3; the wave impedances Z_ν and the wave numbers k_ν are defined in Eqs. (3) and (4) respectively. The matrix T is unimodular ($T_{11}T_{22}-T_{12}T_{21}=1$) for lossless dielectrics, and since k_2, k_3 are real (propagating rather than evanescent waves), then $T_{11}=T_{22}^*$ and $T_{12}=T_{21}^*$. Propagation characteristics of the system are determined via the Floquet theorem [22] by its eigenvalues derived from the condition $|T-e^{-jKL}I|=0$, where K is the Bloch wave number, $L=\Delta_2+\Delta_3$ is the periodicity, and KL is the phase advance per cell. Utilizing the above mentioned qualities of the transition matrix, the eigenvalues are found to be

$$e^{-jKL} = \kappa_{1,2} = \left(\frac{T_{11}+T_{22}}{2}\right) \pm \sqrt{\left(\frac{T_{11}+T_{22}}{2}\right)^2 - 1}, \tag{21}$$

and the corresponding eigenvectors are

$$V_{1,2} = \begin{pmatrix} 1 \\ \frac{\kappa_{1,2} - T_{11}}{T_{12}} \end{pmatrix}. \tag{22}$$

By adding the two eigenvalues we get the dispersion relation

$$\cos(KL) = \frac{1}{2}(T_{11} + T_{22}), \tag{23}$$

implying that field confinement is ensured when the absolute value of the right hand side is larger than unity

$$\left(\frac{T_{11} + T_{22}}{2}\right)^2 > 1. \tag{24}$$

Plugging the explicit expressions for the elements of the matrix T given by Eq. (20) into Eq. (24), we obtain the condition

$$\left(\frac{T_{11} + T_{22}}{2}\right)^2 = \left(\frac{(Z_3 + Z_2)^2}{4Z_3Z_2}\cos(\Psi_3 + \Psi_2) - \frac{(Z_3 - Z_2)^2}{4Z_3Z_2}\cos(\Psi_3 - \Psi_2)\right)^2 > 1. \tag{25}$$

It is evident that for a given set of dielectric coefficients and a given frequency ω_0, extremum occurs for $\Psi_3+\Psi_2=l\pi$, $\Psi_3-\Psi_2=s\pi$, where l and s are integers and $|l-s|$ must be odd. For example, taking each layer to be a quarter of transverse wavelength thick $[\Delta_\nu=\lambda_0/(4\sqrt{\varepsilon_\nu-1}), \nu=2,3]$ or, in other words, assuming $\Psi_3+\Psi_2=\pi$ and $\Psi_3-\Psi_2=0$, we get

$$\left|\frac{T_{11} + T_{22}}{2}\right|_{\max} = \frac{1}{2}\left(\frac{Z_3}{Z_2} + \frac{Z_2}{Z_3}\right). \tag{26}$$

Consequently, the attenuation after n periods is

$$|e^{-jKL}|^n = \begin{cases} \left(\frac{Z_3}{Z_2}\right)^n, & Z_3 < Z_2 \\ \left(\frac{Z_2}{Z_3}\right)^n, & Z_3 > Z_2. \end{cases} \tag{27}$$

The above choice entails that in addition to the frequency ω_0, band gaps of the structure will be created around $\omega=3\omega_0$, $5\omega_0,\cdots$, and so on. This formulation is valid regardless of the angle of incidence of the wave relative to the dielectric discontinuity. In case of a wave impinging perpendicularly upon a planar interface, the impedance is $Z=\eta_0/\sqrt{\varepsilon}$, whereas if the wave has a phase velocity c in the z direction, then the impedance is as given in Eq. (3) $Z=\eta_0\sqrt{\varepsilon-1}/\varepsilon$.

2. Achieving confinement in the PBA

As already indicated, the above description of the confinement process is of an *infinite* Bragg reflector. In case of a *semi-infinite* structure, as in the PBA, the design constraints on the first layer are different. For the perfect reflection to occur, the amplitudes of the outgoing and incoming waves at the entrance to the semi-infinite periodic structure should be in one of the corresponding eigenvectors [Eq. (22)]

$$V_1 = \begin{pmatrix} 1 \\ -1 \end{pmatrix}, \quad V_2 = \begin{pmatrix} 1 \\ 1 \end{pmatrix}. \tag{28}$$

If $Z_3<Z_2$ the first eigenvector is obtained, and E_z achieves an extremum at the entrance to the structure, and if $Z_3>Z_2$ then E_z is zero. In both cases the eigenvalue is the same. Thus, depending on which dielectric material is the *first* in the unit cell of the periodic structure, the longitudinal electric field E_z should either peak or vanish at the entrance to the structure. Moreover, since any discontinuity can be regarded as an entrance to a semi-infinite periodic structure, the aforementioned condition is satisfied at *any* boundary between the two dielectrics. A general condition on the boundary between layer $\nu\neq 0$ and layer $\nu+1$ can therefore be stated as follows:

$$\begin{cases} E_z(x = D_\nu + \Delta_\nu/2) = 0 & \text{if } Z_\nu > Z_{\nu+1}, \\ \dfrac{\partial E_z}{\partial x}(x = D_\nu + \Delta_\nu/2) = 0 & \text{if } Z_\nu < Z_{\nu+1}, \end{cases} \tag{29}$$

and for the discontinuity between the first and the second layers we have

$$\begin{cases} E_z(x = D_{\text{int}} + \Delta_1) = 0 & \text{if } Z_1 > Z_2, \\ \dfrac{\partial E_z}{\partial x}(x = D_{\text{int}} + \Delta_1) = 0 & \text{if } Z_1 < Z_2. \end{cases} \tag{30}$$

That is to say that the first layer should be of such width that at the interface with the next layer, the perfect reflection condition is met. In the first layer the amplitudes are completely determined by D_{int}/λ_0 and ε^{I} according to Eq. (10), or explicitly

$$A_1/E_0 = (B_1/E_0)^* = \frac{1}{2}e^{jk_1D_{\text{int}}} - j\frac{1}{2}\frac{\omega_0}{c}D_{\text{int}}\frac{Z_1}{\eta_0}e^{jk_1D_{\text{int}}}. \tag{31}$$

Given the amplitudes, as required by Eq. (30), it is now straightforward to determine the points where E_z peaks or vanishes according to its expression [Eq. (2)]. The resulting expression for the first layer width reads

$$\Delta_1 = \begin{cases} \dfrac{1}{k_1}\arctan\left(\dfrac{1}{\dfrac{Z_1}{\eta_0}\dfrac{\omega_0}{c}D_{\text{int}}}\right), & Z_1 > Z_2, \\ \dfrac{1}{k_1}\arctan\left(-\dfrac{Z_1}{\eta_0}\dfrac{\omega_0}{c}D_{\text{int}}\right), & Z_1 < Z_2, \end{cases} \tag{32}$$

where the smallest positive value of the arctan function is chosen. With this regard, the first layer may be conceived as a *matching layer* between the vacuum region and the subsequent periodic structure, as it rotates the amplitude vector dictated by the vacuum mode, to overlap the eigenvector of the periodic structure. In the first case of Eq. (32) the resulting electromagnetic field would be identical for $|x|\leqslant D_{\text{int}}+\Delta_1$ if there were metallic walls at $x=\pm(D_{\text{int}}+\Delta_1)$, and the second case is equivalent to perfect magnetic conducting boundaries.

3. Confinement features

Confinement entails vanishing *real* part of the transverse component of the complex Poynting vector, meaning that in each dielectric layer there is a standing wave. Taking E_0 to be real without loss of generality, we get $A_\nu=B_\nu^*$. It is therefore evident that for the structure to truly support the desired mode, there must be an infinite number of layers, otherwise energy would "leak out" and there would be no confinement. In a practical structure, the number of layers should be suf-

ficient so that the outward power flow is negligible. There are a few methods for estimating the losses in Bragg reflection waveguides [6,23,9]. Generally, the overall influence of the transverse finiteness of the structure can be expressed by an imaginary part of the longitudinal wave number k_z.

Figure 4 illustrates a typical spatial distribution of the longitudinal electric field as well as the total electric field for a PBA made of silica ($\varepsilon^{\mathrm{I}}=2.1$) and zirconia ($\varepsilon^{\mathrm{II}}=4$), and $D_{\mathrm{int}}=0.3\lambda_0$. It shows that E_z is uniform in the vacuum layer while oscillating and decaying exponentially in the Bragg layers. Another feature is that E_z vanishes and achieves a maximum alternately at the discontinuities, as discussed previously. Accordingly, the transverse electric field E_x, derived from E_z with respect to x, is maximal and discontinuous whenever E_z is zero, and zero whenever E_z peaks. The total electric field in turn, undergoes a discontinuity every second interface.

Figure 5 illustrates the confinement for two quantities, the longitudinal electric field (E_z) and the longitudinal Poynting vector (S_z) for $D_{\mathrm{int}}=0.3\lambda_0$ at instant $t=0$; the longitudinal component of the electric field is shown in the left frame being normalized to its maximum value on axis, and the longitudinal component of the Poynting vector normalized by $|E_0|^2/\eta_0$ is depicted in the right frame. While the former peaks in the vacuum and is gradually decaying in the transverse direction, the Poynting vector is zero on axis, it increases monotonically to (almost) a peak value at the vacuum-dielectric interface and then decays gradually with oscillations.

In order to illustrate the confinement process in more detail, Fig. 6 presents the variation of the normalized *energy density* in space for the PBA configuration analyzed above. Thus, the magnitude of the electric field vector increases from a local minimum on axis, to a larger value

$$\frac{E_{\max}}{E_0}=\sqrt{1+\left(\frac{2\pi D_{\mathrm{int}}}{\lambda_0}\right)^2} \tag{33}$$

at the vacuum-dielectric discontinuity; for most practical purposes this may also be considered the maximum electric field—a fact revealed also by the bottom frame of Fig. 4. From this value, the field decays exponentially according to the expression in Eq. (27). Assuming, without loss of generality, that the characteristic impedance in the first region is lower than in the second ($Z_1<Z_2$) and for a layer sufficiently away from the center we may approximate the location of the layer in terms of the number of periods $x\simeq nL$, the exponential decay of the electromagnetic energy density is proportional to $(Z_1/Z_2)^{2n}\simeq(Z_1/Z_2)^{2x/L}=e^{-2x/x_c}$ while, in general,

$$x_c=\frac{\lambda_0}{4}\left(\frac{1}{\sqrt{\varepsilon_1-1}}+\frac{1}{\sqrt{\varepsilon_2-1}}\right)\left|\ln\left(\frac{\varepsilon_1\sqrt{\varepsilon_2-1}}{\varepsilon_2\sqrt{\varepsilon_1-1}}\right)\right|^{-1}. \tag{34}$$

Further insight on the field confinement is revealed by the top frames of Fig. 7 illustrating the electric, magnetic and the total energy density across the PBA. While the top-left frame illustrates the exponential decay of the average normalized electromagnetic energy density $[W_{\mathrm{EM}}(x)/W_{\mathrm{EM}}(0)]$ over the cross section of the structure, the top-right one shows a magnified region including the electric as well as the magnetic

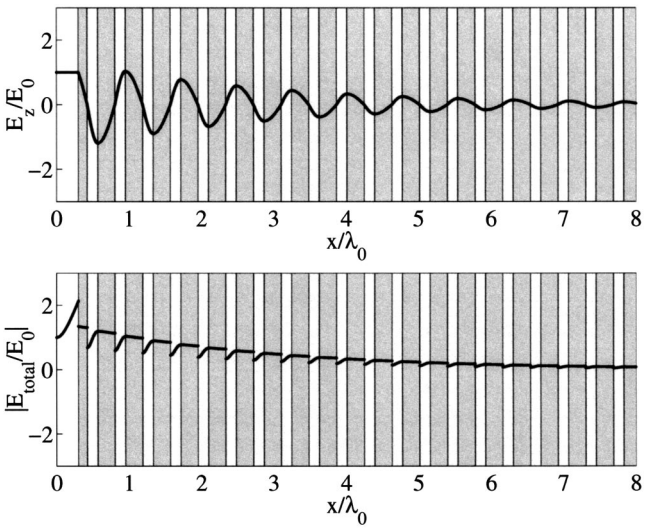

FIG. 4. A typical distribution of the longitudinal electric field (top) and the total electric field (bottom), $D_{\mathrm{int}}=0.3\lambda_0, \varepsilon^{\mathrm{I}}=2.1, \varepsilon^{\mathrm{II}}=4$.

average energy densities. It is evident that the electric energy has a maximum in the first layer, the magnetic energy density vanishes every second discontinuity (since $\partial E_z/\partial x=0$), and it peaks in between where it is also much larger than the electric energy density. When the magnetic field vanishes, the transverse electric field is also zero, and therefore all the energy density is stored in the longitudinal electric field. This picture is even better illustrated by the two bottom frames showing the normalized Poynting vector $S_z(x)/S_z(x=D_{\mathrm{int}})$. It starts from a zero value on axis, it peaks in the first layer, and then it decays exponentially while dropping to zero in each period of the structure; the bottom-right is a magnification of the left frame.

B. CBA Design procedure

A straightforward periodic structure analysis is unsuitable for the case of the CBA, where the curvature of the layers (cylindrical coordinates) changes with the distance from the axis. Nevertheless, some of the results obtained for the PBA presented in the previous section apply to the CBA case as well.

We adopt here an approach given in Ref. [6], and implement it for the design of the CBA. As a starting point consider Eq. (9) which, assuming a given gradient, entail that the amplitudes are determined from the inside out. Let us now assume that the amplitudes in some layer ν are known, and we need to determine the location of the boundary between this layer and the following one $(\nu+1)$ such that the average energy density in the second layer is *minimal*. Keeping in mind that the confinement entails that the amplitudes of the outgoing and incoming waves in each layer are complex conjugates of each other, minimizing the average energy density is equivalent to minimizing the absolute value of the amplitude in layer $\nu+1$. Performing mathematically this optimization process results in the condition

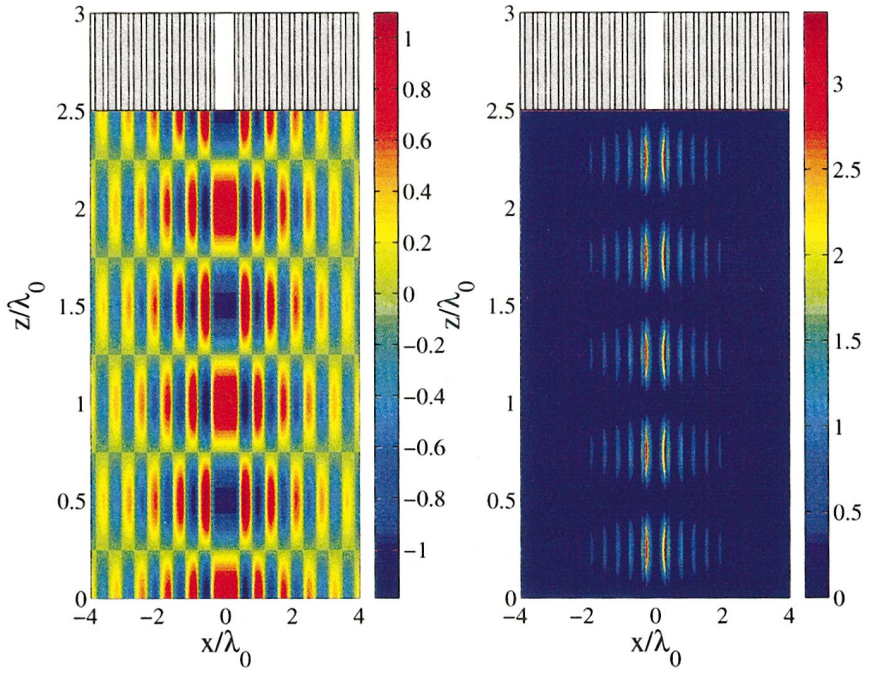

FIG. 5. (Color) Contours of the normalized longitudinal electric field (left) and the Poynting vector (right) at instant $t=0$ ($D_{\text{int}}=0.3\lambda_0, \varepsilon^{\text{I}}=2.1, \varepsilon^{\text{II}}=4$). The dielectric layers are depicted at the top of each frame.

$$\begin{cases} E_z(r=R_\nu+\Delta_\nu/2)=0 & \text{if } Z_\nu > Z_{\nu+1}, \\ \dfrac{\partial E_z}{\partial r}(r=R_\nu+\Delta_\nu/2)=0 & \text{if } Z_\nu < Z_{\nu+1}, \end{cases} \tag{35}$$

which is the same as Eq. (29) obtained for the PBA. Hence, it is possible to design the CBA from the inside out. For a given set of the three parameters, the gradient on axis, the internal radius, and the dielectric coefficient of the first layer, the field distribution is completely determined by Eq. (18). The boundary between the first and the second layer is set to satisty Eq. (35), and then the amplitudes in the second layer are determined, and so forth. The layers are placed sequentially optimally in the sense that confinement is achieved after a minimum number of layers. Apart from the first layer, the above condition is asymptotically equivalent to the "quarter wavelength" condition discussed above since for large arguments the points where the longitudinal electric field reaches maximum or zero are a quarter of wavelength apart. Another manifestation of this condition is that it implies that the radial component of the Poynting vector vanishes at each discontinuity. The design procedure of the CBA is therefore simply a generalization of the one given for the PBA.

An illustration of the distribution of the two quantities S_z and E_z in two cases $R_{\text{int}}=0.3\lambda_0$ (top) and $0.8\lambda_0$ (bottom), is given in Fig. 8; the longitudinal component of the electric field is shown in the left frames being normalized to its value

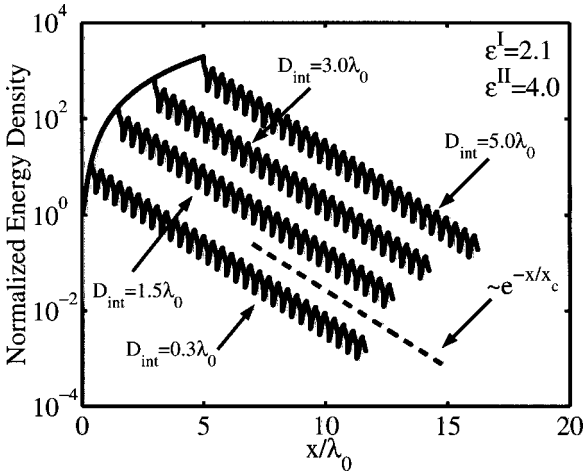

FIG. 6. Normalized energy as a function of the distance from axis x for various values of D_{int}. The dashed line illustrates the analytic expression for the confinement parameter Eq. (34).

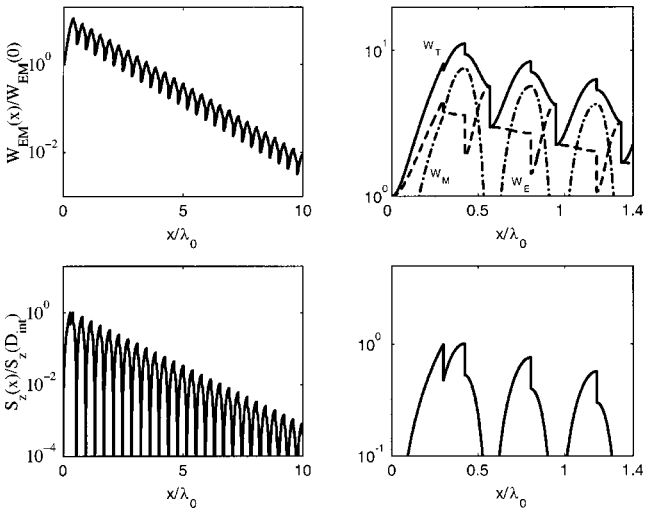

FIG. 7. Normalized energy and normalized longitudinal Poynting vector decay across the structure ($D_{\text{int}}=0.3\lambda_0, \varepsilon^{\text{I}}=2.1, \varepsilon^{\text{II}}=4$). Top left: Normalized total energy. Top right: enlarged interval of the normalized energies, electric, magnetic, and total. Bottom left: normalized longitudinal Poynting vector. Bottom right: enlarged interval of the normalized longitudinal Poynting vector.

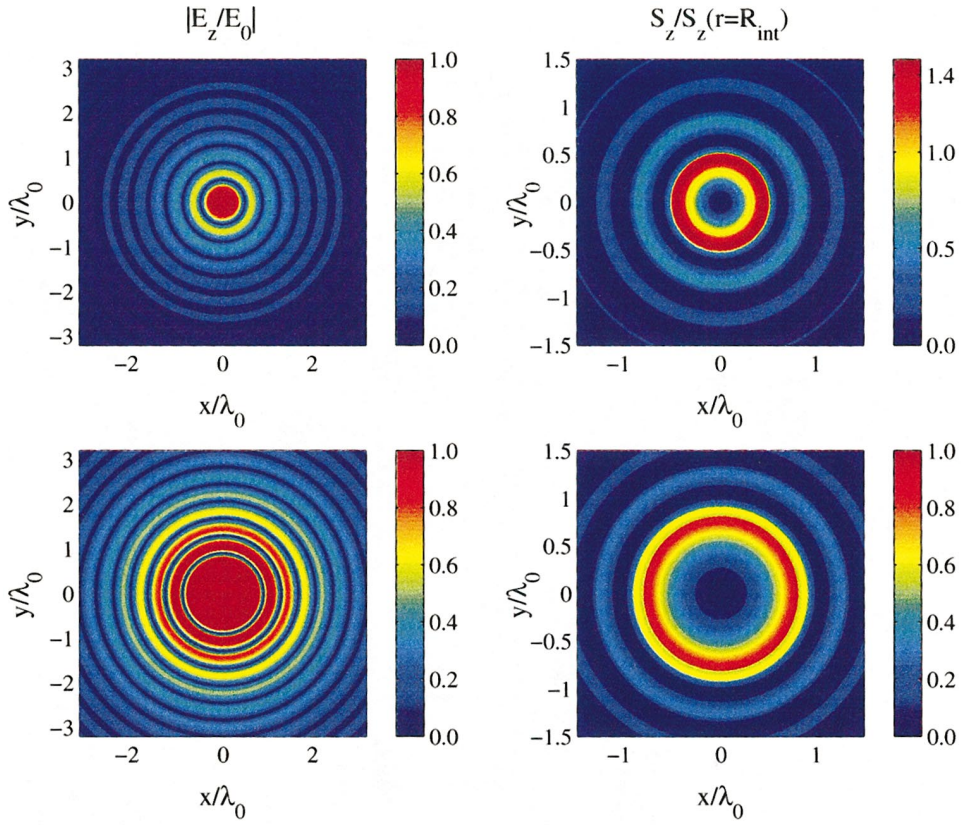

FIG. 8. (Color) CBA ($\varepsilon^{\mathrm{I}}=2.1, \varepsilon^{\mathrm{II}}=4$) contours of normalized longitudinal electric field (left) and Poynting vector (right) in two cases: $R_{\mathrm{int}}=0.3\lambda_0$ (top) and $0.8\lambda_0$ (bottom).

on axis and the longitudinal component of the Poynting vector normalized to its value at the vacuum-dielectric interface is depicted in the right frames. Although the general behavior of the fields across the CBA resembles that of the PBA, there are two differences between the two cases, which are responsible for a stronger confinement in the CBA. The first difference is that in the CBA the decay of the energy across the fiber is not purely exponential, but there is also a factor of $1/r$ because of the Hankel functions. The second difference is that for $R_{\mathrm{int}}=D_{\mathrm{int}}$, the maximum electric field for a given gradient is given by

$$\frac{E_{\max}}{E_0}=\sqrt{1+\left(\pi\frac{R_{\mathrm{int}}}{\lambda}\right)^2}, \tag{36}$$

which is smaller than in the PBA for the same half-width; the difference is that the radial electric field is smaller by a factor of 2 than the transverse electric field in the PBA, as was already pointed out above.

IV. ACCELERATOR PARAMETERS

From the perspective of an acceleration structure there are three significant quantities to be determined: the interaction impedance, the group velocity, and the maximum electric field experienced by the structure.

A. Interaction impedance

The interaction impedance is a measure of the accelerating gradient experienced by the electrons for a given amount of power injected into the system, and it is defined by

$$Z_{\mathrm{int}}\triangleq\frac{|\lambda_0 E_0|^2}{P}. \tag{37}$$

For the PBA, P denotes the flowing power in the z direction per unit length of y, and the interaction impedance has units of $\Omega\ m$, whereas for the CBA, P denotes the total power flowing across the fiber, and the interaction impedance is in Ω. Assuming that the materials' characteristics are known ($\varepsilon=2.1,4.0$) and so is the laser wavelength (λ_0), the only free parameter left is the dimension of the vacuum region. In order to have a rough estimate of its impact, it is possible to obtain an upper limit on the interaction impedance, by considering an idealized situation in which the energy flux outside the vacuum region is negligible. The quantity obtained depends only on the form of the fields in the vacuum core, and on its size. Evaluation of these two upper bounds on the interaction impedance results in

$$Z_{\mathrm{int}}^{(\max)}[\Omega\ m]\triangleq\frac{|\lambda_0 E_0|^2}{P_V}=\frac{\eta_0\lambda_0}{\frac{4}{3\pi}\left(\pi\frac{D_{\mathrm{int}}}{\lambda_0}\right)^3} \tag{38}$$

for the PBA, and the CBA expression reads

$$Z_{\mathrm{int}}^{(\max)}[\Omega]\triangleq\frac{|\lambda_0 E_0|^2}{P_V}=\frac{\eta_0}{\frac{1}{4\pi}\left(\pi\frac{R_{\mathrm{int}}}{\lambda_0}\right)^4}. \tag{39}$$

In both expressions P_V is the power flowing in the vacuum, evaluated by integration over the cross section of the longi-

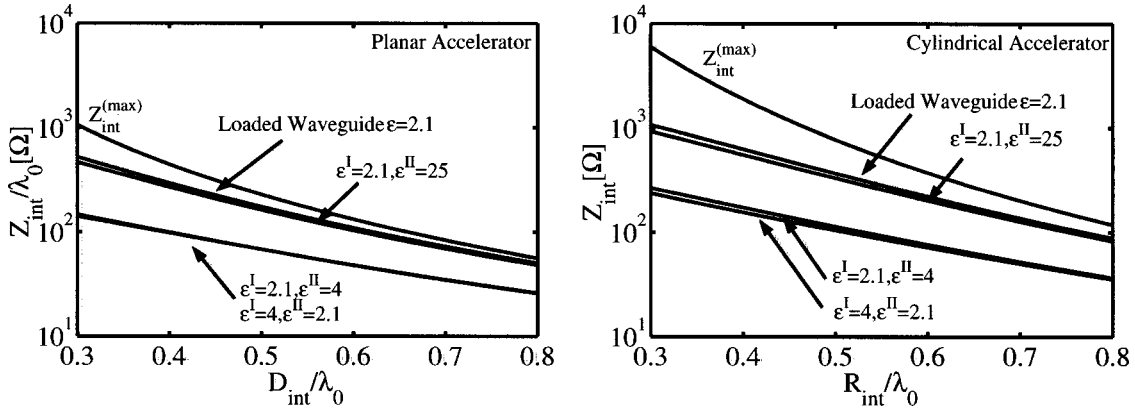

FIG. 9. Interaction impedance as a function of the vacuum core dimension for the PBA (left) and for the CBA (right).

tudinal Poynting vector of the fields given by Eq. (1) for the PBA and Eq. (15) for the CBA. The two above expressions are depicted in Fig. 9 and are the top curves in the left (PBA) and the right (CBA) frames. The bottom two curves in each frame show the exact interaction impedance for two cases: the lowest curve represents the case where the *first* layer is made of a material of higher dielectric coefficient ($\varepsilon^I=4.0$). A similar interaction impedance is achieved if the first layer is made of the material of lower dielectric coefficient ($\varepsilon^I=2.1$). Best fit curves are given for $0.3\leqslant D_{int}/\lambda_0\leqslant 0.8$

$$\frac{Z_{int}}{\eta_0\lambda_0}(\varepsilon^I=2.1,\varepsilon^{II}=4)\simeq 1.124-3.561\left(\frac{D_{int}}{\lambda_0}\right)+4.258\left(\frac{D_{int}}{\lambda_0}\right)^2-1.823\left(\frac{D_{int}}{\lambda_0}\right)^3,$$

$$\frac{Z_{int}}{\eta_0\lambda_0}(\varepsilon^I=4,\varepsilon^{II}=2.1)\simeq 1.020-3.073\left(\frac{D_{int}}{\lambda_0}\right)+3.502\left(\frac{D_{int}}{\lambda_0}\right)^2-1.436\left(\frac{D_{int}}{\lambda_0}\right)^3, \quad (40)$$

for the PBA and for the CBA ($0.3\leqslant R_{int}/\lambda_0\leqslant 0.8$) the best fit is

$$Z_{int}(\varepsilon^I=2.1,\varepsilon^{II}=4)\simeq\frac{1.66\eta_0}{1+\left(3.648\frac{R_{int}}{\lambda_0}\right)^2+\left(2.07\frac{R_{int}}{\lambda_0}\right)^4},$$

$$Z_{int}(\varepsilon^I=4,\varepsilon^{II}=2.1)\simeq\frac{1.48\eta_0}{1+\left(3.7\frac{R_{int}}{\lambda_0}\right)^2+\left(1.95\frac{R_{int}}{\lambda_0}\right)^4}. \quad (41)$$

Although the two bottom curves of the PBA seem to coincide, there is a slight advantage to a lower dielectric coefficient in the first layer up to $D_{int}\simeq 0.5\lambda_0$, starting from which the relation is reversed. In the CBA case there is an obvious advantage to the lower dielectric coefficient in the first layer. Higher contrast between the two materials can significantly increase the interaction impedance, as seen in the third curve from the bottom of Fig. 9 for $\varepsilon=2.1,25$. For comparison, a partially dielectric loaded waveguide ($\varepsilon=2.1$) has an interaction impedance which is almost one order of magnitude larger than that of the silica-zirconia Bragg reflection waveguide (both PBA and CBA), and slightly greater than the $\varepsilon=2.1,25$ structure—still its value is significantly smaller than the value of the upper bound $Z_{int}^{(max)}$.

The importance of using materials with *high dielectric coefficients* is also shown in Fig. 10, which presents the contours of constant interaction impedance for the PBA in the plane of ε^I and ε^{II}. Since no confinement may be expected when the medium is uniform ($\varepsilon^I=\varepsilon^{II}$), this impedance is virtually zero on the diagonal. Similarly, when either one of the dielectrics is close to unity, the thickness of the layer being proportional to $1/\sqrt{\varepsilon-1}$, implies thick layers, large confinement space, and therefore, low interaction impedance. In between these three minima there are two *asymmetric* regions of maximum interaction impedance. As indicated above, the asymmetry is due to the choice of which material consists the first layer. According to this figure, the general trend is that larger impedance may be obtained when the first layer is of lower value. For example, taking for the CBA case $R_{int}=0.3\lambda_0$ we get $Z_{int}(\varepsilon^I=10,\varepsilon^{II}=30)\sim 2500\ \Omega$, whereas $Z_{int}(\varepsilon^I=30,\varepsilon^{II}=10)\sim 2000\ \Omega$. However, this trend changes for a different value of R_{int} (or D_{int}).

Designing the structure for confinement in a minimum number of layers, does not achieve maximum interaction impedance. The attenuation per unit cell of the transverse periodic structure is given in Eq. (27) as a ratio between the two materials' transverse impedances. Maximum attenuation is therefore obtained when choosing one of the dielectric materials to have $\varepsilon=2$, since, as already indicated, the transverse impedance [Eq. (3)] has a maximum for this value. The other dielectric should be as large as possible, or as close as possible to unity. This will indeed create maximum attenuation per unit cell, however, the interaction impedance depends on the total flowing power outside the vacuum layer, which tends to grow when low dielectric coefficient materials are used and the layers become thicker. For instance, choosing one dielectric material to have $\varepsilon=2$ and the other as small as possible would result in high attenuation per period, but very low interaction impedance (see Fig. 10). Conse-

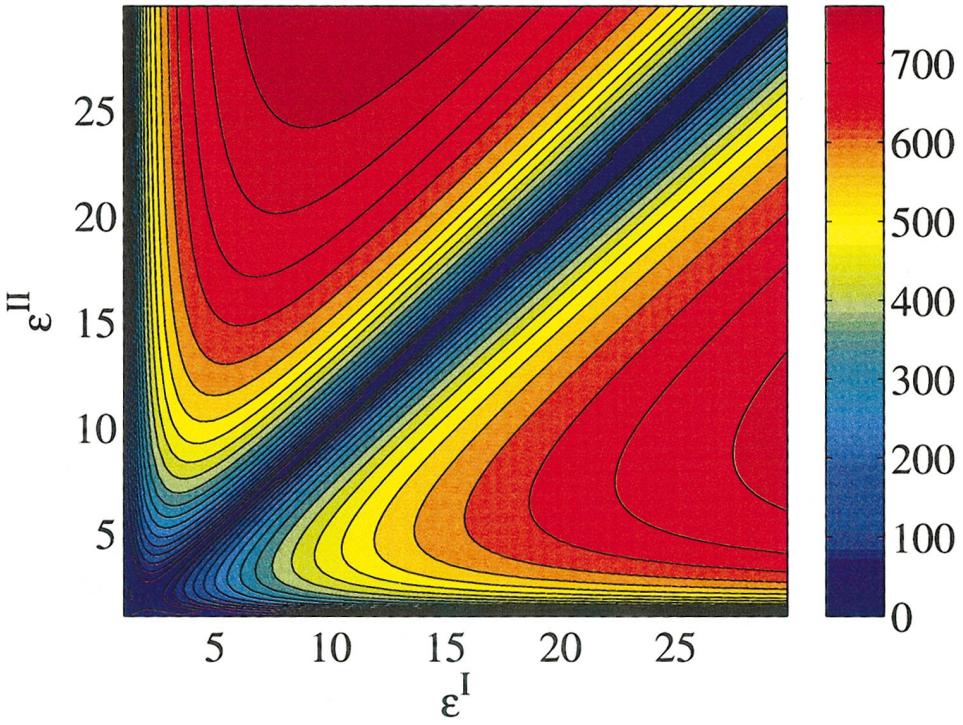

FIG. 10. (Color) Contours of constant interaction impedance $Z_{\mathrm{int}}/\lambda_0[\Omega]$ in the $(\varepsilon^{\mathrm{I}},\varepsilon^{\mathrm{II}})$ plane, with $D_{\mathrm{int}}=0.3\lambda_0$.

quently, there exists a tradeoff between creating high contrast between the two materials, and using low dielectric coefficient materials. This tradeoff is responsible for the pattern seen in Fig. 10, in which for a certain ε^{I} there could he several values of $\varepsilon^{\mathrm{II}}$ for which the interaction impedance has the same value.

B. Energy velocity

A similar approach may be adopted for the analysis of the energy velocity, which generally equals the group velocity [24], and in this case it is of the first TM mode in the structure at $k_z=\omega_0/c$.

Defining for the PBA the time average energy per unit area as $W_{\mathrm{EM}}\triangleq\int_{-\infty}^{\infty}dx\, w_{\mathrm{EM}}(x)$, where w_{EM} is the energy density, or for the CBA $W_{\mathrm{EM}}\triangleq 2\pi\int_0^{\infty}dr\, rw_{\mathrm{EM}}(r)$ per unit length, the energy velocity reads

$$\frac{v_{\mathrm{EN}}}{\mathrm{c}}\triangleq\frac{P}{cW_{\mathrm{EM}}}. \tag{42}$$

The energy velocity illustrated in Fig. 11 may be approximated by a best fit for the PBA ,

$$\frac{v_{\mathrm{EN}}}{c}(\varepsilon^{\mathrm{I}}=2.1,\varepsilon^{\mathrm{II}}=4)\simeq 0.342+0.290\left(\frac{D_{\mathrm{int}}}{\lambda_0}\right)-0.061\left(\frac{D_{\mathrm{int}}}{\lambda_0}\right)^2,$$

$$\frac{v_{\mathrm{EN}}}{c}(\varepsilon^{\mathrm{I}}=4,\varepsilon^{\mathrm{II}}=2.1)\simeq 0.305+0.326\left(\frac{D_{\mathrm{int}}}{\lambda_0}\right)-0.068\left(\frac{D_{\mathrm{int}}}{\lambda_0}\right)^2. \tag{43}$$

A best fit for the CBA energy velocity is given by

$$\frac{v_{\mathrm{EN}}}{c}(\varepsilon^{\mathrm{I}}=2.1,\varepsilon^{\mathrm{II}}=4)\simeq 0.379+0.0079\left(\frac{R_{\mathrm{int}}}{\lambda_0}\right)+0.065\left(\frac{R_{\mathrm{int}}}{\lambda_0}\right)^2,$$

$$\frac{v_{\mathrm{EN}}}{c}(\varepsilon^{\mathrm{I}}=4,\varepsilon^{\mathrm{II}}=2.1)\simeq 0.350+0.0060\left(\frac{R_{\mathrm{int}}}{\lambda_0}\right)+0.09\left(\frac{R_{\mathrm{int}}}{\lambda_0}\right)^2, \tag{44}$$

and clearly, the choice of the dielectric in the first layer has some effect although not significant.

Before we proceed it is instructive to point out the relation of a parameter frequently quoted in (microwave) accelerators' literature, namely, the R/Q of the structure (R being the shunt impedance and Q the quality factor) to the parameters presented above. Specifically, in case of a standing wave structure it is shown in Appendix A that $R/Q\simeq\beta_{\mathrm{EN}}Z_{\mathrm{int}}/(2\pi\lambda_0)$.

C. Maximum electric field

The last parameter of interest is the maximum field sustained by the structure before breakdown. For avoiding breakdown it is assumed that the fluence threshold of the material given by [25]

$$F[\mathrm{J/cm^2}]=\begin{cases}1.44\tau_p^{1/2}, & \tau_p\,[\mathrm{psec}]>10,\\ 2.51\tau_p^{1/4}, & 0.4<\tau_p\,[\mathrm{psec}]<10,\\ 2, & \tau_p\,[\mathrm{psec}]<0.4,\end{cases}$$

where τ_p is the pulse duration, limits the maximum field to about 2 GV/m. For example, taking $\varepsilon^{\mathrm{I}}=4, v_{\mathrm{EN}}=0.6c$ and $\tau_p<0.4$ psec, the maximal field is given by [26] $E_{\max}=\sqrt{F/(0.5\varepsilon_0\varepsilon^{\mathrm{I}}v_{\mathrm{EN}}\tau_p)}\simeq 2.5$ GV/m. Therefore, bearing in

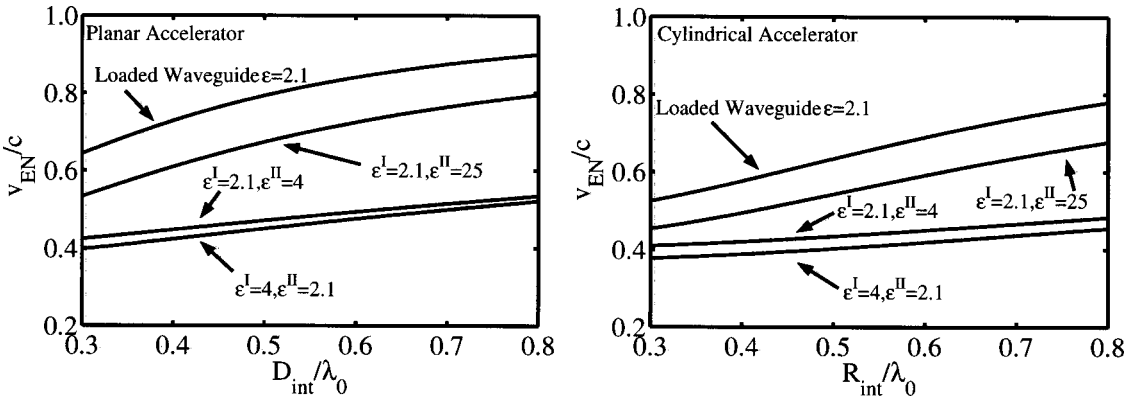

FIG. 11. Energy velocity as a function of the vacuum core dimension for the PBA (left) and for the CBA (right).

mind that the gradient of interest is of the order of 1 GV/m [26], then according to Eq. (33) the half-width of the vacuum core in the PBA needs to be no larger than

$$\frac{E_{\max}}{E_0} = 2 \Rightarrow D_{\text{int}} \simeq 0.28\lambda_0 \tag{45}$$

and according to Eq. (36) for the CBA

$$\frac{E_{\max}}{E_0} = 2 \Rightarrow R_{\text{int}} \simeq 0.55\lambda_0. \tag{46}$$

As already discussed, the CBA is less vulnerable to breakdown, and the maximum internal radius allowed is twice as much the internal half-width D_{int} for the same gradient. In Table I (PBA) and Table II (CBA) a few typical values of interest are presented for $\varepsilon^{\text{I}}=2.1$ and $\varepsilon^{\text{II}}=4$ implying that $x_c \simeq 2.68\lambda_0$ and $L=0.38\lambda_0$.

V. WAKE-FIELD ANALYSIS

The last topic that needs to be considered in the present study is an estimate of the wake field generated by a train of microbunches in such a dielectric structure. In a recent study [21] a general formulation of the wake field for an arbitrary dielectric structure with a cylindrical vacuum tunnel was given. Based on this formulation, we next determine the (symmetric) wake field of a line charge moving in a general planar structure, and obtain analytical results for some simple cases. Results for the Bragg structures, both the PBA and the CBA are given.

A. Wake field in the PBA

The current density of a line charge in free space, infinite in y and moving in the z direction with a constant velocity v is given by

$$J_z(x,z,t) = -q' v\,\delta(x)\,\delta(z-vt), \tag{47}$$

wherein $(-q')$ is the charge per unit length. The electromagnetic field can be derived from the nonhomogeneous wave equation of the magnetic vector potential (Lorentz gauge)

$$\left[\nabla^2 - \frac{1}{c^2}\frac{\partial^2}{\partial t^2}\right] A_z(x,z,t) = -\mu_0 J_z(x,z,t). \tag{48}$$

In Appendix B the solution of the wave equation is formulated dividing the electromagnetic field into two contributions. The field generated by the line charge in free space is called the primary field, and the remainder, which is due to the effect of the surrounding structure, is called the secondary field. Assuming that the material adjacent to the vacuum region has a dielectric coefficient ε^{I}, it is convenient to define the relation between the outgoing and incoming waves just outside the vacuum tunnel as a function of frequency $\mathbb{R}(\omega)$. This reflection coefficient is directly dependent on the surrounding layers and their dielectric constants.

For the case $\mathbb{R} \equiv 0$, i.e., a vacuum tunnel within a homogeneous material with ε^{I}, the secondary field is evaluated to obtain the decelerating field on the moving line charge

$$\mathcal{E}_{\parallel} \triangleq E_z^{(s)}(x=0,z=vt,t) = \frac{-q'}{2\pi\varepsilon_0 D_{\text{int}}} \times \text{Re}\left\{ j \ln\left(1 + j\frac{\gamma\sqrt{\beta^2\varepsilon^{\text{I}} - 1}}{\varepsilon^{\text{I}}}\right)\right\}. \tag{49}$$

It is evident that below the Cerenkov velocity $(v=c/\sqrt{\varepsilon^{\text{I}}})$, the decelerating force is zero. It increases monotonically with the velocity, and for the ultrarelativistic regime $(\gamma \to \infty)$ the decelerating field

TABLE I. Exact parameters of the PBA for several internal half-widths of the vacuum; the materials are $\varepsilon^{\text{I}}=2.1$ and $\varepsilon^{\text{II}}=4$ implying that $x_c \simeq 2.68\lambda_0$ and a structure periodicity $L=0.38\lambda_0$.

	$D_{\text{int}}=0.3\lambda_0$	$D_{\text{int}}=0.4\lambda_0$	$D_{\text{int}}=0.45\lambda_0$	$D_{\text{int}}=0.5\lambda_0$	$D_{\text{int}}=0.55\lambda_0$
$Z_{\text{int}}/\lambda_0[\Omega]$	147.13	99.230	81.87	67.94	56.77
β_{EN}	0.424	0.448	0.460	0.471	0.483
$E_{\max}/E_0$	2.134	2.705	2.999	3.297	3.598

TABLE II. Exact parameters of the CBA for several internal radii of the vacuum tunnel; the materials are $\varepsilon^{\mathrm{I}}=2.1$ and $\varepsilon^{\mathrm{II}}=4$ implying that $r_c \simeq 2.68\lambda_0$ and for a ("planar") structure period $L=0.38\lambda_0$.

	$R_{\mathrm{int}}=0.3\lambda_0$	$R_{\mathrm{int}}=0.4\lambda_0$	$R_{\mathrm{int}}=0.45\lambda_0$	$R_{\mathrm{int}}=0.5\lambda_0$	$R_{\mathrm{int}}=0.55\lambda_0$
$Z_{\mathrm{int}}[\Omega]$	267.46	173.73	140.62	114.27	93.29
β_{EN}	0.410	0.420	0.427	0.434	0.442
$E_{\max}/E_0$	1.374	1.606	1.732	1.862	1.996

$$\mathcal{E}_{\parallel} = \frac{q'}{2\pi\varepsilon_0 D_{\mathrm{int}}}\frac{\pi}{2}, \tag{50}$$

is $\pi/2$ times the radial field of a static line charge at distance D_{int}. Although this expression was calculated for a simple structure consisting of a vacuum core in an otherwise uniform dielectric, in case of an ultrarelativistic line charge it is valid also if the structure has surrounding layers [21]. Causality arguments may be shown to lead to the conclusion that reflections caused by such layers reach the axis only after the original source has moved away. In other words, the reacting (decelerating) field on an ultrarelativistic particle itself is *independent* of the details of the structure layers, and it depends only on the charge and the size of the vacuum core.

From here on we shall focus on the ultrarelativistic regime, and it is demonstrated in Appendix B that the expression for the longitudinal electric field within the vacuum tunnel is independent of x and is given by the inverse Fourier transform integral

$$E_z^{(s)}(\overline{\tau}) = \frac{q'}{2\pi\varepsilon_0 D_{\mathrm{int}}}\frac{1}{2}\int_{-\infty}^{\infty} d\overline{\omega} e^{j\overline{\omega\tau}}\frac{1+\mathbb{R}}{(1+j\overline{\omega})-(1-j\overline{\omega})\mathbb{R}}, \tag{51}$$

where $\overline{\omega}\triangleq\omega\sqrt{\varepsilon^{\mathrm{I}}-1}D_{\mathrm{int}}/(\varepsilon^{\mathrm{I}}c)$ is the normalized frequency and $\overline{\tau}$ is the normalized space-time such that $\overline{\omega\tau}=\omega(t-z/v)$. Moreover, the fields outside the vacuum tunnel within the *first* dielectric layer are similarly given by

$$E_z^{(s)}(x,\overline{\tau}) = \frac{q'}{2\pi\varepsilon_0 D_{\mathrm{int}}}\frac{1}{2}\int_{-\infty}^{\infty} d\overline{\omega} e^{j\overline{\omega\tau}}\frac{1}{(1+j\overline{\omega})-(1-j\overline{\omega})\mathbb{R}} \times[e^{-j\Lambda(x-D_{\mathrm{int}})}+\mathbb{R}e^{j\Lambda(x-D_{\mathrm{int}})}], \tag{52}$$

where $\Lambda\triangleq|\overline{\omega}|\varepsilon^{\mathrm{I}}/D_{\mathrm{int}}$.

Describing explicitly the electromagnetic field reflected from the layers of the PBA, it is necessary to resort to the transition matrix formulation developed in Sec. II [Eq. (20)] subject to similar constraints of wave number [Eq. (4)] and transverse impedance [Eq. (3)], since an ultrarelativistic particle imposes $k_z \simeq \omega/c$. If we assume a finite PBA structure comprised of n periods ($N=2n$ layers), using the eigenvalues and eigenvectors of the transition matrix, the total transition is found to be

$$\mathcal{L}\triangleq T^n = \begin{pmatrix} 1 & 1 \\ \dfrac{\kappa_1 - T_{11}}{T_{12}} & \dfrac{\kappa_2 - T_{11}}{T_{12}} \end{pmatrix}\begin{pmatrix} \kappa_1^n & 0 \\ 0 & \kappa_2^n \end{pmatrix} \times\begin{pmatrix} \dfrac{\kappa_2 - T_{11}}{T_{12}} & -1 \\ \dfrac{T_{11}-\kappa_1}{T_{12}} & 1 \end{pmatrix}\frac{T_{12}}{\kappa_2-\kappa_1}. \tag{53}$$

Taking into account the effect of the first layer, which as explained above is not part of the periodic structure, the reflection coefficient reads

$$\mathbb{R} = -\frac{\mathcal{L}_{21}}{\mathcal{L}_{22}} e^{-2j(\omega/c)\sqrt{\varepsilon^{\mathrm{I}}-1}\,\Delta_1} = \frac{1}{T_{12}}\frac{(\kappa_1^n-\kappa_2^n)(\kappa_1-T_{11})(\kappa_2-T_{11})}{\kappa_1^n(\kappa_1-T_{11})-\kappa_2^n(\kappa_2-T_{11})} e^{-2j(\omega/c)\sqrt{\varepsilon^{\mathrm{I}}-1}\,\Delta_1}. \tag{54}$$

Given the reflection coefficient as a function of frequency, the wake field can be computed numerically according to Eq. (51). For a specific geometry, $N=50$ layers, $D_{\mathrm{int}}=0.3\lambda_0$, $\varepsilon^{\mathrm{I}}=2.1$, and $\varepsilon^{\mathrm{II}}=4$, the reflection coefficient is depicted in Fig. 12.

Analytic expressions for the ultrarelativistic wake field can be obtained for some simple cases. For the case $\mathbb{R}\equiv 0$ the wake field in the vacuum tunnel (51) is easily evaluated to show exponential decay behind the moving charge, or explicitly

$$E_z^{(s)} = \frac{q'}{2\pi\varepsilon_0 D_{\mathrm{int}}}\pi e^{-(t-z/c)\varepsilon^{\mathrm{I}}c/(D_{\mathrm{int}}\sqrt{\varepsilon^{\mathrm{I}}-1})}u(t-z/c), \tag{55}$$

where $u(t)$ is the unit step function defined by

$$u(t)\triangleq\begin{cases} 0, & t<0, \\ 0.5, & t=0, \\ 1, & t>0. \end{cases} \tag{56}$$

Hence, for $t=z/c$ we obtain once again Eq. (50). For comparison with the PBA we shall also consider a partially *dielectric loaded* planar transmission line with either metallic ($\sigma\to\infty$) or perfect magnetic ($\mu_r\to\infty$) boundaries. The vacuum tunnel will have the same width as the PBA, and the dielectric layer width is set so that the structure supports the fundamental mode for the laser frequency ω_0. This condition is equivalent to determining the first layer in the PBA, expressed explicitly in Eq. (32), where the case $Z_1>Z_2$ is analogous to the metallic case, and $Z_1<Z_2$ to the magnetic

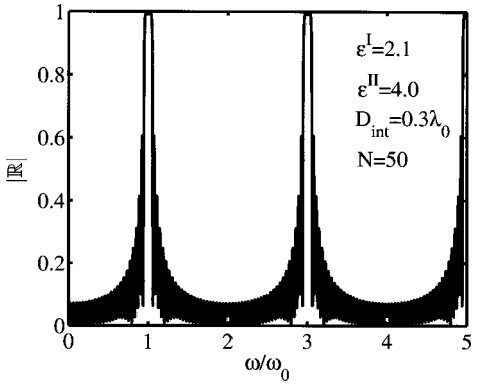

FIG. 12. Absolute value of the reflection coefficient as a function of the frequency.

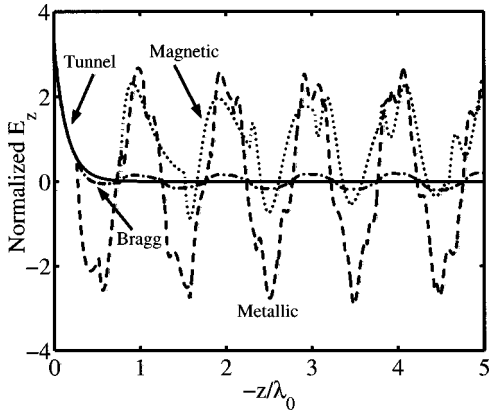

FIG. 13. A snapshot of the longitudinal wake field E_z normalized by $q'/(2\pi\varepsilon_0 D_{\rm int})$ at time $t=0$ of a vacuum tunnel ($\mathbb{R}\equiv 0$), PBA, and partially dielectric loaded metallic as well as perfect magnetic transmission lines. In all cases $\varepsilon^{\rm I}=2.1$, and the PBA has $\varepsilon^{\rm II}=4$. For the first region all four curves coincide.

walls case. Evaluation of the longitudinal wake field for the metallic transmission line is given in Ref. [14]. In Appendix C it is shown that the formulation presented here results in the same expression given by

$$E_z^{(s)} = \frac{q'}{2\pi\varepsilon_0 D_{\rm int}} \sum_i \frac{\pi}{1+\frac{a}{2}\sin^{-2}\left(\frac{a\overline{\omega_i}}{2}\right)} \cos[\omega_i(t-z/c)] \times u(t-z/c), \tag{57}$$

wherein $a \triangleq 2\varepsilon^{\rm I}\Delta_1/D_{\rm int}$, and the frequencies $\overline{\omega_i}$ are solutions of $\cot(a\overline{\omega}/2)=\overline{\omega}$. A similar expression is given in Appendix C for the magnetic wall case.

In Fig. 13 a snapshot of the wake field at $t=0$ (the charge is at $z=0$) is given for the $\mathbb{R}\equiv 0$ case, the PBA case with $N=10$, and the partially dielectric loaded metallic and magnetic transmission lines. In all cases the material surrounding the vacuum tunnel has $\varepsilon^{\rm I}=2.1$, and in the PBA the second material has $\varepsilon^{\rm II}=4$. Due to this choice, the width of the metallic transmission line is the same as that of the PBA, and different than that of the perfect magnetic transmission line.

Governed by causality, the reflections from the transverse discontinuities contribute, each in its turn, to the wake field observed within the vacuum tunnel. All four curves *coincide* for some distance behind the moving charge, starting from the decelerating field value (50) for $z=0$, jumping to twice that value for $z=0^-$ and then decaying exponentially. Since the transverse wave number for all waves is $k_x=(\omega/c)\sqrt{\varepsilon-1}$, it is evident that the transverse group velocity is $c/\sqrt{\varepsilon-1}$ in each material. Therefore, taking into account the charge velocity $v\cong c$, the first reflection in the PBA or the metallic transmission line is observable in the vacuum layer at a distance $2\Delta_1\sqrt{\varepsilon^{\rm I}-1}$ behind the charge, and both of these curves become separated at this point from the other two. Contributions from farther layers in the PBA are then seen to affect the vacuum wake field every $\lambda_0/2$, and reflections from the metallic walls affect the wake field in this case every $2\Delta_1\sqrt{\varepsilon^{\rm I}-1}$. Similarly, the curve for the magnetic wall transmission line is separated from the $\mathbb{R}\equiv 0$ case according to its first layer width, which is larger than that of the metallic wall and the PBA, and therefore occurs behind them. From the above discussion it can be concluded that due to causality, for example, the wake field of a PBA with $N>10$ is exactly the same as the $N=10$ wake field for the interval shown, as the more distant layers do not *yet* influence the field in the vacuum core. An interpretation of the the wake-field as a sum of lossy modes in the PBA is given in Appendix C. Comparison between the metallic wall transmission line and the PBA can also be seen in Fig. 14, where a picture in the *x*-*z* plane of the two longitudinal wake fields is given.

B. Emitted power in the PBA

It was discussed above that the decelerating force on a single ultrarelativistic charge does not depend on the surrounding structure. In practice the *macrobunch* of a future optical acceleration structure may consist of a train of $M(\sim 1000)$ microbunches separated by a wavelength (λ_0) of the driving laser field. On pure acceleration grounds, in order to maintain a reasonable energy spread, the typical bunch length ought to be smaller than $\lambda_0/12$. Typically, the first discontinuity has no effect on the leading microbunch since referring to the previous causality discussion, the first effect occurs only after a distance $2\Delta_1\sqrt{\varepsilon^{\rm I}-1}$ behind the front of the microbunch. The expression for the first layer width [Eq. (32)] implies that $\Delta_1 \leqslant \lambda_0/(4\sqrt{\varepsilon^{\rm I}-1})$, so that the first reflection reaches the axis at a distance smaller than $\lambda_0/2$ behind the charge. Although the total power in case of a single microbunch is not affected by the PBA, the field spatial distribution trailing the particle is obviously strongly affected, and so is the power emitted by the train of micro-bunches, as will be discussed next.

Let us consider $N_{\rm LC}$ ultrarelativistic line charges, each having charge per unit length $q'_{\rm LC}$, divided into M microbunches, as shown in Fig. 15. An estimate for the emitted power per unit length assuming that all the charge is located in a single microbunch ($M=1$) is given by Eq. (50)

$$P_1 = \frac{v}{2\pi\varepsilon_0 D_{\rm int}} \frac{\pi}{2} (N_{\rm LC} q'_{\rm LC})^2. \tag{58}$$

On the other hand, if the $N_{\rm LC}$ line charges are randomly distributed such that the average field they generate is zero,

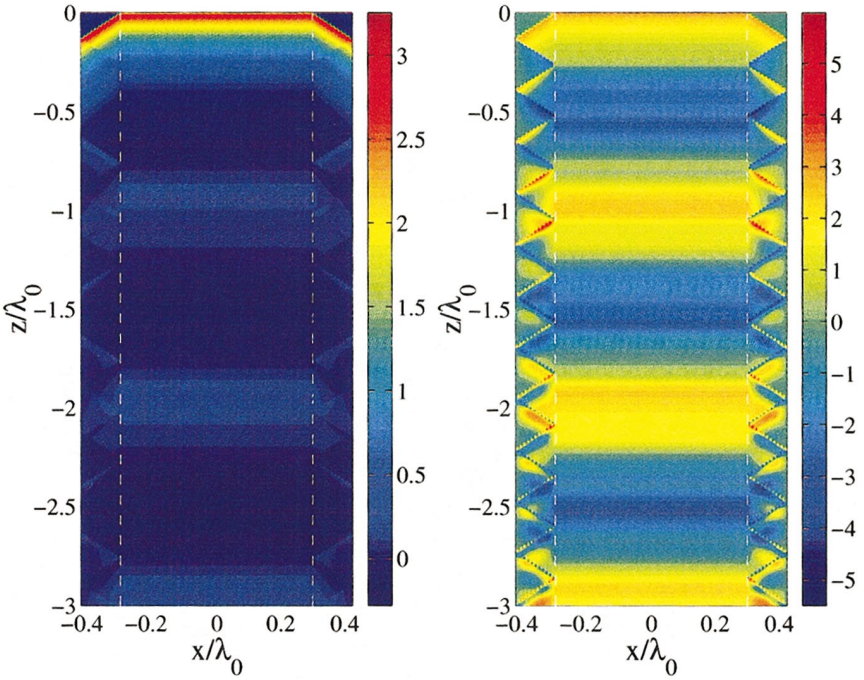

FIG. 14. (Color) A snapshot of the longitudinal wake field E_z normalized by $q'/(2\pi\varepsilon_0 D_{\text{int}})$ at time $t=0$ of the PBA (left), and a partially dielectric loaded metallic transmission line (right). Both cases have $\varepsilon^{\text{I}}=2.1$, and the PBA has $\varepsilon^{\text{II}}=4$.

then the total emitted power is N_{LC} times the power emitted by a single line charge, i.e.,

$$P_{N_{\text{LC}}} = \left[\frac{v}{2\pi\varepsilon_0 D_{\text{int}}}\frac{\pi}{2}(q'_{\text{LC}})^2\right]N_{\text{LC}}. \tag{59}$$

A qualitative expression for $M \geqslant 1$ may be evaluated for the case of a "weak mirror" ($\mathbb{R}\sim 0$), by neglecting the effects of the microbunches on each other. In this case the total power is M times the power of one microbunch of charge $N_{\text{LC}}q'_{\text{LC}}/M$, which results in

$$P = \left[\frac{v}{2\pi\varepsilon_0 D_{\text{int}}}\frac{\pi}{2}\left(\frac{N_{\text{LC}}q'_{\text{LC}}}{M}\right)^2\right]M = \frac{P_1}{M}. \tag{60}$$

With the exception of D_{int}, the last expression is virtually independent of the parameters of the structure, and it describes best the case where the vacuum core is surrounded with homogeneous material, i.e., there are no dielectric layers. The expression in Eq. (60) exhibits two limiting cases, bearing in mind that $1 \leqslant M \leqslant N_{\text{LC}}$: for a single microbunch ($M=1$) the emitted power $P=P_1$ is maximal, and if M $=\mathrm{N_{LC}}$ the emitted power $P=P_1/N_{\text{LC}}$ is minimal. The last expression is valid also in the case when the line charges are *randomly* distributed, and the mutual average effect is zero, as discussed before. Clearly Eq. (60) represents both the regimes of "spontaneous" as well as the "stimulated" emission of radiation of N_{LC} line charges.

In Appendix D it is shown that the electromagnetic power generated by a microbunch of total charge per unit length q' distributed to M microbunches, each one being $\lambda_0(\alpha/2\pi)$ long, is given by

$$P = \frac{v(q')^2}{2\pi\varepsilon_0 D_{\text{int}}}\frac{1}{2}\int_{-\infty}^{\infty} d\bar{\omega}\frac{1+\mathbb{R}}{(1+j\bar{\omega})-(1-j\bar{\omega})\mathbb{R}} \times\left\{\operatorname{sinc}\left[\frac{\alpha}{2}\frac{\bar{\omega}}{\bar{\omega}_0}\right]\frac{\operatorname{sinc}\left[\pi\dfrac{\bar{\omega}}{\bar{\omega}_0}M\right]}{\operatorname{sinc}\left[\pi\dfrac{\bar{\omega}}{\bar{\omega}_0}\right]}\right\}^2, \tag{61}$$

where $\operatorname{sinc}(x)\equiv\sin(x)/x$ and $\bar{\omega}$ is as defined before. Simulations indicate that if $0\leqslant\alpha<\pi/2$ the power is virtually independent of α and within a good approximation it is inversely proportional to M. Figure 16 (left) illustrates the normalized power $\bar{P}\triangleq P(v(q'_{\text{LC}})^2N_{\text{LC}}^2/2\pi\varepsilon_0 D_{\text{int}})^{-1}$ for a PBA with $N=10$, 20, 30, 40, and for the no-reflections case. It shows that for a stronger confinement (large N) the power emitted is higher, but is more moderately dependent on the number of bunches. For a small number of bunches, it is seen that the general behavior is $\sim 1/M$ in correspondence to Eq. (60). Similarly to the wake-field curves previously discussed, the power curve coincide for small M's, and split one at a time, the curves of less layers first. The point where a curve splits

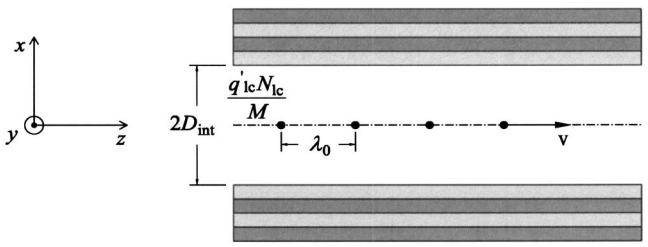

FIG. 15. A macrobunch consisting of a train of microbunches. N_{LC} line charges, each having q'_{LC} amount of charge are arranged in M microbunches.

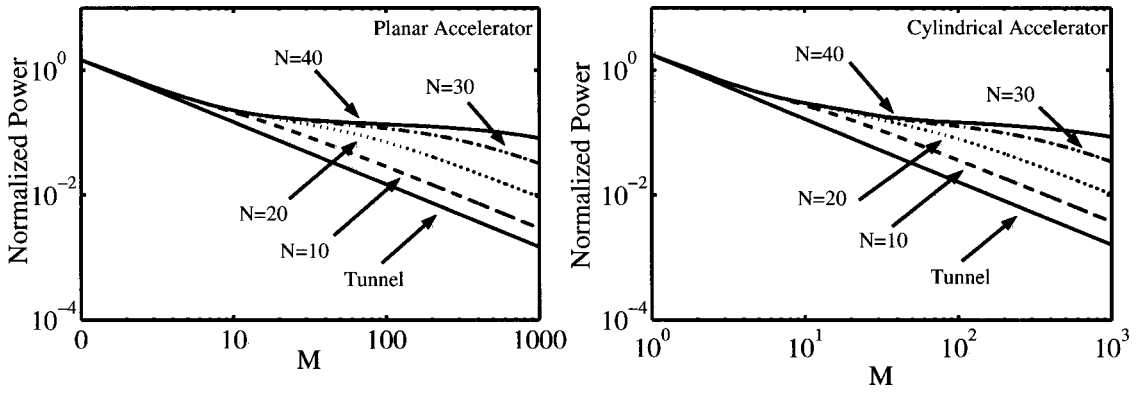

FIG. 16. Normalized power generated by a train of M microbunches ($D_{\mathrm{int}}=0.3\lambda_0, \varepsilon^{\mathrm{I}}=2.1, \varepsilon^{\mathrm{II}}=4$) for the PBA (left) and for the CBA with $R_{\mathrm{int}}=0.3\lambda_0$ (right).

from the higher N curves is the point behind the first microbunch where the transverse finiteness of the structure is first felt. Following the transverse path of the waves emitted from the particle, we find that the time it takes for the waves to be reflected from the $N+1$ discontinuity (not including the vacuum-dielectric interface) assuming N is even, is

$$\Delta t_N = \frac{2\Delta_1}{v_x^{\mathrm{I}}} + \frac{N}{2}\left(\frac{2\Delta_2}{v_x^{\mathrm{II}}} + \frac{2\Delta_3}{v_x^{\mathrm{I}}}\right) = \frac{2\Delta_1\sqrt{\varepsilon^{\mathrm{I}}-1}}{c} + \frac{N}{2}\frac{\lambda_0}{c}, \tag{62}$$

wherein $v_x^{\mathrm{I}} \triangleq c/\sqrt{\varepsilon^{\mathrm{I}}-1}$ and $v_x^{\mathrm{II}} \triangleq c/\sqrt{\varepsilon^{\mathrm{II}}-1}$ are the transverse group velocities in each material. It is sufficient to consider only the widths of the second and third layers ($\Delta_{2,3}$) since the rest of the layers are periodic with the same quarter of transverse wavelength thickness $\lambda_0/(4\sqrt{\varepsilon-1})$. As the particle moves, for all practical purposes, at the speed of light c, the distance this reflection occurs behind it is $\Delta t_N c$. Keeping in mind that the microbunches are one wavelength apart, the number of microbunches for which a curve splits from the higher N curves is therefore given by rounding up $\Delta t_N c$ divided by λ_0, or explicitly

$$M_N = \left\lceil 2\frac{\Delta_1}{\lambda_0}\sqrt{\varepsilon^{\mathrm{I}}-1} + N/2 \right\rceil + 1. \tag{63}$$

A significant difference between the PBA and *closed* structures is seen in Fig. 17, where the curves for $N=50, 80, 120$, as well as the curves for the metallic and the magnetic wall structures are plotted. The curves of $N=80$ and $N=120$ almost coincide, indicating that this is the limiting curve when the number of layers is increased. In the closed structure case, the emitted power is of the form (see Appendix D)

$$P = \frac{(q')^2 v}{2\pi\varepsilon_0 D_{\mathrm{int}}}\frac{\pi}{2}\sum_i W_i \,\mathrm{sinc}^2\left(\frac{\alpha}{2}\frac{\overline{\omega_i}}{\overline{\omega_0}}\right)\frac{\mathrm{sinc}^2\left[\pi\dfrac{\overline{\omega_i}}{\overline{\omega_0}}M\right]}{\mathrm{sinc}^2\left(\pi\dfrac{\overline{\omega_i}}{\overline{\omega_0}}\right)}. \tag{64}$$

Unlike the two top curves of the magnetic and metallic cases, the PBA allows for energy to escape out of the structure through the propagation bands (see reflection coefficient in Fig. 12), the trailing bunches are less affected by the wake field, and hence the emitted power is smaller. This clearly reveals the significant advantage of a PBA over any other closed structure.

C. Wake field and emitted power in the CBA

Analysis of the wake field in the CBA is quite similar to the analysis presented above for the PBA with a few minor differences. For the CBA the secondary force on axis for an ultrarelativistic charge $(-q)$ is [21]

$$E_z^{(s)} = \frac{q}{4\pi\varepsilon_0 R_{\mathrm{int}}^2}\left[\frac{2}{\pi}\int_{-\infty}^{\infty} d\overline{\omega}\frac{1+\mathbb{R}(\overline{\omega})}{\psi + j\overline{\omega} - (\psi^* - j\overline{\omega})\mathbb{R}(\overline{\omega})}e^{j\overline{\omega}\overline{\tau}}\right], \tag{65}$$

the angular frequency being normalized according to $\overline{\omega} = (\omega R_{\mathrm{int}}/c)\sqrt{\varepsilon-1}/(2\varepsilon)$ unlike the PBA case, the normalized delay is $\overline{\tau} = (t-z/c)(c/R_{\mathrm{int}})(2\varepsilon)/\sqrt{\varepsilon-1}$; $\psi(\overline{\omega}) \equiv -jH_1^{(2)}(2\overline{\omega}\varepsilon)/H_0^2(2\overline{\omega}\varepsilon)$ and for large arguments $\psi(\overline{\omega} \gg 1) \simeq 1$. The power emitted by a single point charge is

$$P = \frac{vq^2}{4\pi\varepsilon_0 R_{\mathrm{int}}^2} \times 2, \tag{66}$$

and the qualitative analysis detailed above for the case of a "weak mirror" applies here as well. Similarly to Eq. (61), the emitted power expression is given by

$$P = \frac{vq^2}{4\pi\varepsilon_0 R_{\mathrm{int}}^2}\frac{2}{\pi}\int_{-\infty}^{\infty} d\overline{\omega}, \frac{1+\mathbb{R}(\overline{\omega})}{\psi + j\overline{\omega} - (\psi^* - j\overline{\omega})\mathbb{R}(\overline{\omega})} \times \mathrm{sinc}^2\left(\frac{\alpha}{2}\frac{\overline{\omega}}{\overline{\omega_0}}\right)\frac{\mathrm{sinc}^2\left[\pi M\dfrac{\overline{\omega}}{\overline{\omega_0}}\right]}{\mathrm{sinc}^2\left(\pi\dfrac{\overline{\omega}}{\overline{\omega_0}}\right)}, \tag{67}$$

and it is illustrated in the right hand frame of Fig. 16 revealing great resemblance to the PBA; in this case the power is normalized to $P \triangleq P(vq_{\mathrm{el}}^2 N_{\mathrm{el}}^2/4\pi\varepsilon_0 R_{\mathrm{int}}^2)^{-1}$, where N_{el} is the number of electrons and q_{el} is the electron charge. As opposed to the PBA case, where an analytic expression for the

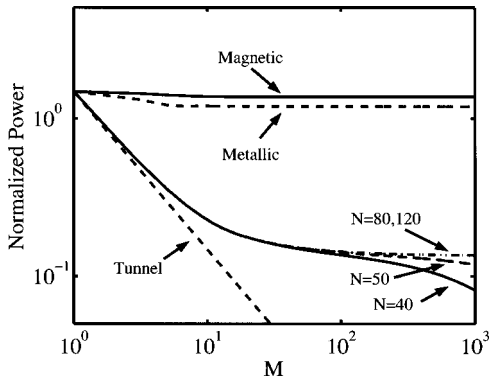

FIG. 17. Normalized power generated by a train of M microbunches ($D_{\mathrm{int}}=0.3\lambda_0, \varepsilon^{\mathrm{I}}=2.1, \varepsilon^{\mathrm{II}}=4$) for the PBA.

reflection coefficient is available, computation of the refection coefficient is performed by utilizing the matrix formulation presented in Sec. II B

VI. DISCUSSION

In the present study we have designed and analyzed a hollow-fiber acceleration structure based on a Bragg reflector consisting of a series of lossless dielectric layers. It is anticipated that their inherent symmetry provides a significant advantage, in what regards emittance growth, over the two-dimensional photonic band gap structure that supports a nonsymmetric field in the axis region or planar metallic structures with similar properties [26]. Conceptually, by analogy to an optical fiber, for confining an electromagnetic wave around a vacuum tunnel ($\varepsilon=1$), it is necessary to ensure that at the operating frequency the effective dielectric coefficient of the surrounding material is smaller than unity ($\varepsilon<1$). In fact, it is convenient to distinguish between three main regions: the vacuum tunnel, on the one hand, and the "periodic mirror", on the other, are the two straightforward regions consistent with the optical fiber view. However, we have found that the third important region is the first layer which does not have to be of the same dimensions as either one of the other layers. Its role is actually to match (electromagnetically) between the "vacuum region mode" and the eigenmode of the periodic structure. The resulting mode is equivalent to having either metallic or perfect magnetic boundaries around the first layer at the operating frequency. In this study it was indeed shown that a Bragg structure can support a mode with longitudinal wave number $k_z=\omega/c$, as required for acceleration purposes. Extending this approach to *cylindrical* layers [Eq. (35)], a better confinement was found relative to the PBA because of the additional $1/r$ transverse energy decay, and because the total field is smaller at the vacuum-dielectric interface. In either the CBA or the PBA structure, if the wave impinges upon the mirror perpendicularly each layer must be a quarter of wavelength thick $\lambda_0/(4\sqrt{\varepsilon})$, whereas in our case the wave has a significant component parallel to the reflection plane ($k_z=\omega/c$), and therefore, the thickness of each layer has to be $\lambda_0/(4\sqrt{\varepsilon-1})$. From the manufacturing perspective this leads to the conclusion that the effectively lower dielectric coefficients ($\varepsilon-1$) entail a larger number of layers for achieving good reflection in comparison to the case of a perpendicularly impinging wave.

Relevant acceleration parameters have been investigated and it was found that for parameters, corresponding to zirconia ($\varepsilon=4$) and silica ($\varepsilon=2.1$), the interaction impedance varies [Eqs. (40) and (41)] between 20 and about 265 Ω for the CBA, according to the internal radius of the vacuum tunnel. In case of the PBA, the interaction impedance per wavelength varies between 25 and 150 Ω. It was shown that with regards to confinement in a minimum number of layers, best results are achieved by choosing one layer with $\varepsilon=2$ and the other as high as possible. However, the interaction impedance is not maximal for this choice as seen in Fig. 10. Most importantly, it was demonstrated that if the other dielectric is as high as $\varepsilon>25$, the interaction impedance reaches values of about 1000 Ω for the CBA; clearly this material needs to sustain intense electric fields and facilitate construction of the submicron dielectric layers in good contact with silica.

Another parameter of interest is the energy velocity [Eqs. (43) and (44)]. For the parameters mentioned above ($\varepsilon=2.1,4$) the energy velocity varies between $0.38c$ and $0.48c$ for the CBA according to the internal radius—Fig. 11. For the PBA the variation is between $0.42c$ to $0.53c$. A third parameter of interest is the maximum field sustained by the structure before the probability of breakdown becomes significant. Since for most practical purposes the maximum field may be assumed to occur at the vacuum-dielectric interface, this quantity may be evaluated analytically—Eqs. (33) and (36). Moreover, if we assume a gradient of 1 GV/m and that the fluence [25] imposes a maximum electric field of 2 GV/m, then the maximum internal radius allowed is $0.55\lambda_0$ for the CBA, and $0.28\lambda_0$ for the PBA.

Within the framework of the mode propagation analysis, two additional important analytic results have been shown explicitly: first an explicit expression for the necessary *thickness* of the first layer in the PBA, Δ_1, was established [Eq. (32)] in terms of the size of the vacuum tunnel and the operating frequency. Secondly, the *confinement parameter* [Eq. (34)] describing the exponential decay of the field in the periodic structure has been established in terms of the dielectric coefficients and the operating wavelength.

In the second part of this study, we examined the electromagnetic wake field and the power generated by a train of microbunches in both the PBA as well as the CBA case. The total emitted power was demonstrated to be limited by two extreme cases. The *lower limit* is set by the power emitted by a train of bunches moving along a vacuum tunnel bored in a dielectric medium that extends to infinity. In this case any radiation generated by a given bunch is emitted outwards, and it practically does not affect trailing bunches. Although there is a nonzero wake on axis, its influence on trailing bunches is negligible, as the wake decays exponentially. In this configuration (or for a small number of layers) the emitted power was found to be proportional to the square of the number of electrons in the macrobunch (N_{el}), and inversely proportional to the number of microbunches ($M<N_{\mathrm{el}}$). This power is also inversely proportional to the square of the internal radius of the structure for the CBA, and to the width of

the vacuum core in thc PBA. The *upper limit* corresponds to a closed structure, namely, a dielectric loaded waveguide where the size of the tunnel is identical to the previous case, and the dielectric layer is set so that at the operating wavelength the mode has phase velocity c. The ideal metal (or perfect magnetic wall) at the boundary, causes all the Cerenkov radiation emitted by the particles to be reflected back to the axis, and as a result there is a significant impact on trailing microbunches. The power emitted by the Bragg structure is between these two limits since there are frequency ranges in which the radiation is confined, whereas for others, the electromagnetic energy leaks out without affecting trailing bunches.

In addition to the pass-band structure of the Bragg layers, the power generated by a macrobunch is determined by the macrobunch's length, the radial extent of the structure, and the causality of the reflections reaching the axis. For example, if there are only a few microbunches (say 5) but many layers, radiation reflected by all the layers which are beyond say 10 layers (beyond $r\sim 2\lambda_0$ for the silica-zirconia structure) will not affect the trailing microbunches. As a result of this causality threshold [Eq. (63)], the power emitted by a macrobunch in a Bragg structure was shown to be significantly different than that emitted in a closed structure. Systematically, the former is lower than the latter.

ACKNOWLEDGMENTS

This study was supported by the Israeli Science Foundation and the United States Department of Energy. At the early stages of this study we benefited from fruitful discussions with R. H. Siemann.

APPENDIX A: THE RELATION OF R/Q TO Z_{int} AND v_{EN}

For deriving the relation between R/Q and Z_{int}, v_{EN}, it is assumed that the relative dielectric coefficient where the wave propagates is of the form $\varepsilon=\varepsilon_r-j\varepsilon_i$, and the loss tangent is given by

$$\tan\,\delta \triangleq \frac{\varepsilon_{\mathrm{i}}}{\varepsilon_r}=\frac{\sigma}{\omega\varepsilon_0\varepsilon_r}, \tag{A1}$$

where σ is the effective conductivity. The dissipated power density is

$$p_D=\frac{1}{2}\sigma\vec{E}^*\cdot\vec{E}=\frac{2\omega_0\varepsilon_i}{\varepsilon_r}\,w_{\mathrm{E}}=2\omega_0\tan\delta\, w_{\mathrm{E}}, \tag{A2}$$

where w_{E} is the time average electric energy density. Further assuming that the loss tangent is approximately identical in all the dielectric materials comprising the structure, the dissipated power per unit length of z is given by

$$P_{\mathrm{D}}=2\omega_0\tan\,\delta\int\int da\, w_{\mathrm{E}}=2\omega_0\tan\delta\, W_{\mathrm{E}} \tag{A3}$$

where W_{E} is the time average energy per unit length. Next, Eq. (A3) is substituted in the definition of the shunt impedance to obtain

$$Z_{\mathrm{shunt}}\triangleq\frac{|E_0|^2}{-dP/dz}=\frac{|E_0|^2}{P_{\mathrm{D}}}=\frac{|E_0|^2}{2\omega_0\tan\delta\, W_{\mathrm{E}}}, \tag{A4}$$

wherein P is the flowing power in the z direction. In a similar way, the quality factor reads

$$Q\triangleq\frac{\omega_0 W_{\mathrm{EM}}}{P_{\mathrm{D}}}=\frac{W_{\mathrm{EM}}}{2\,\tan\delta\, W_{\mathrm{E}}} \tag{A5}$$

where W_{EM} is the time average energy per unit length. Finally, using the definitions of the interaction impedance (37) and the energy velocity (42), the ratio between the shunt impedance (denoted by R) and the quality factor takes the form

$$R/Q=\frac{|E_0|^2}{\omega_0 W_{\mathrm{EM}}}=\frac{\beta_{\mathrm{EN}}Z_{\mathrm{int}}}{2\pi\lambda_0}, \tag{A6}$$

where $\beta_{\mathrm{EN}}=v_{\mathrm{EN}}/c$.

APPENDIX B: FORMULATION OF THE WAKE FIELD IN A PLANAR STRUCTURE

The starting point in establishing the wake-field in a planar structure is to realize that the electromagnetic field generated by the current density (47) in free space, namely the primary field, is given by

$$A_z^{(p)}(x,z,t)=-\frac{q'\mu_0}{4\pi}\int_{-\infty}^{\infty}d\omega\; e^{j\omega(t-z/v)}\frac{1}{\Gamma}e^{-\Gamma|x|}, \tag{B1}$$

where $\Gamma\triangleq|\omega|/c\gamma\beta$. Since the line charge is moving in a vacuum core of a dielectric structure where the material adjacent to the vacuum region has a dielectric coefficient ε^{I}, the effect of the surrounding structure is referred to as the secondary field, and its form is dictated by the primary field to be

$$A_z^{(s)}(x,z,t)=-\frac{q'\mu_0}{4\pi}\int_{-\infty}^{\infty}d\omega\; e^{\,j\omega(t-z/v)}\frac{1}{\Gamma}\times\begin{cases}A_0\cosh(\Gamma x), & |x|<D_{\mathrm{int}},\\ -\dfrac{\varepsilon^{\mathrm{I}}}{\gamma^2\beta^2\overline{\varepsilon}}(C_0e^{-j\Lambda x}+D_0e^{j\Lambda x}), & x>D_{\mathrm{int}},\end{cases} \tag{B2}$$

where $\Lambda\triangleq(|\omega|/c)\sqrt{\varepsilon^{\mathrm{I}}-\beta^{-2}}$ and $\overline{\varepsilon}\triangleq\varepsilon^{\mathrm{I}}-\beta^{-2}$. This solution of the wave equation is assumed to hold only in the first layer adjacent to the vacuum region, and due to the symmetry, it is sufficient to consider only one side of the dielectric structure. The reflections from the surrounding structure are represented by the amplitude D_0.

Based on Eq. (B1) it is possible to establish the electric scalar potential Φ using the Lortenz gauge. Derived from both potentials we obtain the primary fields in the vacuum region $|x|<D_{\mathrm{int}}$

$$E_z^{(p)}(x,z,t)=-\frac{q'\mu_0}{4\pi}\int_{-\infty}^{\infty}d\omega\; e^{\,j\omega(t-z/v)}\left(\frac{j\omega}{\gamma^2\beta^2}\right)\frac{1}{\Gamma}e^{-\Gamma|x|},$$

$$H_y^{(p)}(x,z,t) = -\frac{q'\mu_0}{4\pi}\int_{-\infty}^{\infty} d\omega\, e^{j\omega(t-z/v)}\frac{1}{\mu_0}e^{-\Gamma|x|}\mathrm{sgn}(x). \tag{B3}$$

In a similar way, the secondary fields within the vacuum core are

$$E_z^{(s)}(x,z,t) = -\frac{q'\mu_0}{4\pi}\int_{-\infty}^{\infty} d\omega\, e^{j\omega(t-z/v)}\left(\frac{j\omega}{\gamma^2\beta^2\Gamma}\right)A_0\cosh(\Gamma x), \tag{B4}$$

$$H_y^{(s)}(x,z,t) = -\frac{q'\mu_0}{4\pi}\int_{-\infty}^{\infty} d\omega\, e^{j\omega(t-z/v)}\frac{(-1)}{\mu_0}A_0\sinh(\Gamma x),$$

and the secondary fields for $|x|>D_{\mathrm{int}}$ are

$$E_z^{(s)}(x,z,t) = -\frac{q'\mu_0}{4\pi}\int_{-\infty}^{\infty} d\omega\, e^{j\omega(t-z/v)}\left(\frac{j\omega}{\gamma^2\beta^2\Gamma}\right)\times(C_0e^{-j\Lambda x}+D_0e^{j\Lambda x}),$$

$$H_y^{(s)}(x,z,t) = -\frac{q'\mu_0}{4\pi}\int_{-\infty}^{\infty} d\omega\, e^{j\omega(t-z/v)}\left(-\frac{j\varepsilon^{\mathrm{I}}\Lambda}{\mu_0\gamma^2\beta^2\overline{\varepsilon}\Gamma}\right)\times(C_0e^{-j\Lambda x}+D_0e^{j\Lambda x}). \tag{B5}$$

It is possible to establish a relation between the outgoing and incoming waves in the first dielectric layer in terms of the geometry of the rest of the structure. Explicitly, this is described by

$$\mathbb{R} \triangleq \frac{D_0}{C_0}\,e^{2j\Lambda D_{\mathrm{int}}}, \tag{B6}$$

implying that $\mathbb{R}$ is the reflection coefficient just outside the vacuum tunnel, and it depends on the layers arbitrary configuration. Imposing the continuity of E_z and H_y on the vacuum-dielectric interface, the solution for the amplitudes in the vacuum region is

$$A_0 = \frac{2(1-\zeta\rho)}{e^{2\Gamma D_{\mathrm{int}}}(1+\zeta\rho)-(1-\zeta\rho)}, \tag{B7}$$

where $\zeta \triangleq -j\varepsilon^{1}/\gamma\beta\sqrt{\overline{\varepsilon}}$ and $\rho \triangleq 1-\mathbb{R}/1+\mathbb{R}$.

For the case $\mathbb{R}\equiv 0$, i.e., a vacuum tunnel within a homogeneous material with ε^{I}, the secondary field is next evaluated to obtain the decelerating field on the moving line charge. Beginning with the expression Eq. (B4) and substituting into it Eq. (B7) and $t-z/c=0$ we get

$$\mathcal{E}_{\parallel} \triangleq E_z^{(s)}(x=0,z=vt,t) = \frac{-q'\mu_0}{2\pi}\frac{c}{\gamma\beta}2\,\mathrm{Re}\left\{j\int_0^{\infty} d\omega\frac{1}{\left(\frac{1+\zeta\rho}{1-\zeta\rho}\right)e^{2\Gamma D_{\mathrm{int}}}-1}\right\}. \tag{B8}$$

Since $\mathbb{R}\equiv 0$, we have $\rho=1$, and using the relation

$$\int_0^{\infty} dx\frac{1}{ae^{bx}-1} = \frac{1}{b}\ln\frac{a}{a-1}, \tag{B9}$$

Eq. (49) is obtained. An expression for the longitudinal electric field in the ultrarelativistic regime can be derived from the secondary field Eqs. (B4) and (B7) by replacing $e^{2\Gamma D_{\mathrm{int}}}$ with the two leading terms in the Taylor series and then taking the limit $\gamma\to\infty$, resulting in Eqs. (51) and (52).

APPENDIX C: WAKE FIELD IN TERMS OF THE STRUCTURE EIGEN MODES

The expression of the ultrarelativistic wake field into the accelerating structure eigenmodes is discussed in what follows. It is first instructive to rewrite Eq. (51) as

$$E_z^{(s)} = \frac{q'}{2\pi\varepsilon_0 D_{\mathrm{int}}}\frac{1}{2}\int_{-\infty}^{\infty} d\overline{\omega}e^{j\overline{\omega\tau}}\frac{1}{\frac{1-\mathbb{R}(\overline{\omega})}{1+\mathbb{R}(\overline{\omega})}+j\overline{\omega}} \tag{C1}$$

The denominator in the integrand is denoted by

$$F(\overline{\omega}) \triangleq \frac{1-\mathbb{R}(\overline{\omega})}{1+\mathbb{R}(\overline{\omega})}+j\overline{\omega}. \tag{C2}$$

This is in fact the dispersion function for $k_z=\omega/c$, such that zeros of this function (poles of the integrand) are eigenfrequencies of the structure. Should this function satisfy the conditions for the residue theorem to hold, it is possible to write the above integral as a sum of the eigenmodes or, explicitly,

$$E_z^{(s)} = \frac{q'}{2\pi\varepsilon_0 D_{\mathrm{int}}}\frac{1}{2}\sum_i 2\pi j\frac{1}{F'(\overline{\omega_i})}e^{j\overline{\omega_i\tau}}, \tag{C3}$$

where the prime denotes derivative with respect to $\overline{\omega}$ and $\overline{\omega_i}$ are the zeros of $F(\overline{\omega})$.

In case of a metallic partially loaded transmission line, the reflection coefficient is $\mathbb{R}=-e^{-ja\overline{\omega}}$ where $a \triangleq 2\varepsilon^{\mathrm{I}}\Delta_1/D_{\mathrm{int}}$, and the dispersion function is

$$F(\overline{\omega}) = -j\,\cot(a\overline{\omega}/2)+j\overline{\omega}. \tag{C4}$$

All poles of the integrand are on the $\mathrm{Im}\{\overline{\omega}\}=0$ axis on the complex $\overline{\omega}$ plane. Based on the causality requirement, for $\overline{\tau}>0$ the integration is carried out in a path enclosing the upper half complex plane, including the poles, whereas for $\overline{\tau}<0$ the result is zero. On the moving charge itself $\overline{\tau}=0$, the integral is therefore the average of these two values. Exploiting the complex conjugate symmetry of the dispersion function, the resulting wake field is of the form

$$E_z^{(s)} = \frac{q'}{2\pi\varepsilon_0 D_{\mathrm{int}}}\pi\sum_i W_i\cos(\overline{\omega_i\tau})u(\overline{\tau}), \tag{C5}$$

where W_i are weights given by

$$W_i = \frac{2}{1+\frac{a}{2}\sin^{-2}\left(\frac{a\overline{\omega_i}}{2}\right)} \tag{C6}$$

and

$$\sum_i W_i = 1. \tag{C7}$$

In the dielectric layer ($|x| > D_{\mathrm{int}}$) of the metallic wall transmission line it can be shown in a similar manner that the longitudinal wake field reads

$$E_z^{(s)} = \frac{q'}{2\pi\varepsilon_0 D_{\mathrm{int}}} \pi \sum_i W_i \frac{\sin[\Lambda_i(D_{\mathrm{ext}} - x)]}{\sin[\Lambda_i(D_{\mathrm{ext}} - D_{\mathrm{int}})]} \cos(\overline{\omega_i \tau})\, u(\overline{\tau}), \tag{C8}$$

where $D_{\mathrm{ext}} \triangleq D_{\mathrm{int}} + \Delta_1$. Implementing the same method to the magnetic wall transmission line we get for the dispersion function

$$F(\overline{\omega}) = j \tan(a\overline{\omega}/2) + j\overline{\omega} \tag{C9}$$

and the wake field inside the vacuum core has the expression

$$E_z^{(s)} = \frac{q'}{2\pi\varepsilon_0 D_{\mathrm{int}}} \pi \left[\frac{2}{1 + \frac{a}{2}} + \sum_i \frac{1}{1 + \frac{a}{2}\cos^{-2}\left(\frac{a\overline{\omega_i}}{2}\right)} \cos(\overline{\omega_i \tau}) \right] \times u(\overline{\tau}). \tag{C10}$$

When the structure is not bounded by metallic or perfect magnetic walls, energy can escape. In the simplest case $\mathbb{R} \equiv 0$, the dispersion function has one zero in $\overline{\omega} = j$, which results in an exponential decay [see Eq. (55)], which is consistent with the above formulation. In Fig. 18 the function $\log_{10}|F(\omega)|$ is plotted in the complex plane showing that for a structure that has a Bragg reflector of one period ($n=1$) there are poles that have an imaginary part, indicated by the dark spots (zeros of the dispersion function). Adding more periods to the structure ($n=2,3,4$), it is seen that more poles are added, representing the additional reflections. It is therefore possible to represent the wake field in a Bragg structure as a sum of the residues, meaning that the wake field is given by an infinite sum of lossy modes. An analytic expression for the residues is easily obtained by substituting the Bragg reflection coefficient Eq. (54) into the dispersion function, and performing the derivative.

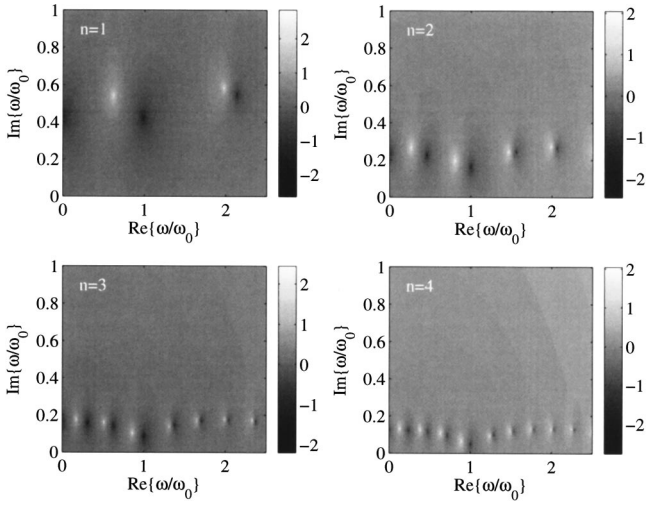

FIG. 18. The dispersion function $\log_{10}|F(\omega)|$ for number of periods $n=1,2,3,4 (N=2n)$. The dark areas indicate zeros of the function which are poles of the wake-field integrand.

APPENDIX D: POWER EMITTED BY A TRAIN OF MICROBUNCHES

Our goal here is to determine the power generated by a train of M microbunches of a relative length $(\alpha/2\pi)\lambda_0$. In the case of a single particle the wake on axis is given by Eq. (51), and this may be extended to include the effect of many particles

$$E(\overline{\tau}) = \frac{1}{2\pi\varepsilon_0 D_{\mathrm{int}}} \times \left[\frac{1}{2} \int_{-\infty}^{\infty} d\overline{\omega} \frac{1 + \mathbb{R}(\overline{\omega})}{1 + j\overline{\omega} - (1 - j\overline{\omega})\mathbb{R}(\overline{\omega})} \sum_i q_i' e^{j\overline{\omega}(\overline{\tau} - \overline{\tau_i})} \right]. \tag{D1}$$

q_i' stands for the charge of the ith particle and $\overline{\tau_i}$ represents its "delay" in the macrobunch relative to some arbitrary reference, e.g., the macrobunch front. Consequently, the power emitted by the macrobunch is

$$P = v \sum_i q_i' E(\overline{\tau} - \overline{\tau_i}) = \frac{v}{2\pi\varepsilon_0 D_{\mathrm{int}}} \times \left[\frac{1}{2} \int_{-\infty}^{\infty} d\overline{\omega} \frac{1 + \mathbb{R}(\overline{\omega})}{1 + j\overline{\omega} - (1 - j\overline{\omega})\mathbb{R}(\overline{\omega})} \left| \sum_i q_i' e^{j\overline{\omega\tau_i}} \right|^2 \right]. \tag{D2}$$

The last term may be simplified subject to two assumptions: (i) there are M microbunches and (ii) each microbunch has a relative length $(\alpha/2\pi)\lambda_0$, thus

$$\sum_i q_i' e^{j\overline{\omega\tau_i}} = \frac{q'}{M} \sum_{\nu=0}^{M-1} \frac{1}{\alpha} \int_{2\pi\nu-\alpha/2}^{2\pi\nu+\alpha/2} d\chi e^{j\frac{\overline{\omega}}{\overline{\omega_0}}\chi} = \frac{q'}{M} \mathrm{sinc}\left(\frac{\alpha}{2}\frac{\overline{\omega}}{\overline{\omega_0}}\right) \sum_{\nu=0}^{M-1} e^{2\pi\nu j \frac{\overline{\omega}}{\overline{\omega_0}}} = q' \mathrm{sinc}\left(\frac{\alpha}{2}\frac{\overline{\omega}}{\overline{\omega_0}}\right) \frac{\mathrm{sinc}\left[\pi M \frac{\overline{\omega}}{\overline{\omega_0}}\right]}{\mathrm{sinc}\left(\pi \frac{\overline{\omega}}{\overline{\omega_0}}\right)} e^{j\pi(M-1)\frac{\overline{\omega}}{\overline{\omega_0}}}, \tag{D3}$$

where q' is the total charge. Substituting in Eq. (D2) we finally obtain

$$P = \frac{v(q')^2}{2\pi\varepsilon_0 D_{\text{int}}}\left\{\frac{1}{2}\int_{-\infty}^{\infty} d\overline{\omega}\frac{1+\mathbb{R}(\overline{\omega})}{1+j\overline{\omega}-(1-j\overline{\omega})\mathbb{R}(\overline{\omega})} \times \text{sinc}^2\left(\frac{\alpha}{2}\frac{\overline{\omega}}{\overline{\omega}_0}\right)\frac{\text{sinc}^2\left[\pi M\dfrac{\overline{\omega}}{\overline{\omega}_0}\right]}{\text{sinc}^2\left(\pi\dfrac{\overline{\omega}}{\overline{\omega}_0}\right)}\right\} \tag{D4}$$

for the power emitted by M microbunches separated by one wavelength of the fundamental frequency.

If the structure under consideration is closed such that the wake field of a single line charge is given as a sum of propagating modes (C5), then the previous expression has poles on the integration path. In this case the total power will be formulated slightly differently, beginning with a sum over all charges and all the contributing modes, given by

$$P = \frac{v}{2\pi\varepsilon_0 D_{\text{int}}}\sum_{\mu} q'_{\mu}\sum_{\nu} q'_{\nu}\pi\sum_{i} W_i \times\cos[\overline{\omega}_i(\overline{\tau}_{\nu}-\overline{\tau}_{\mu})]u(\overline{\tau}_{\nu}-\overline{\tau}_{\mu}), \tag{D5}$$

which can be reformulated in terms of average contributions

$$P = \frac{(q')^2 v}{2\pi\varepsilon_0 D_{\text{int}}}\,\pi\sum_i W_i \times\left\langle\left\langle\cos\left[\frac{\overline{\omega}_i}{\overline{\omega}_0}(\chi_{\mu}-\chi_{\nu})\right]u(\chi_{\mu}-\chi_{\nu})\right\rangle_{\nu}\right\rangle_{\mu}, \tag{D6}$$

wherein χ is the relative phase on the scale of the fundamental angular frequency. In what follows it will be demonstrated that

$$\left\langle\left\langle\cos\left[\frac{\overline{\omega}_i}{\overline{\omega}_0}(\chi_{\mu}-\chi_{\nu})\right]u(\chi_{\mu}-\chi_{\nu})\right\rangle_{\nu}\right\rangle_{\mu} = \frac{1}{2}\,\text{sinc}^2\left(\frac{\alpha}{2}\frac{\overline{\omega}_i}{\overline{\omega}_0}\right)\frac{\text{sinc}^2\left[\pi\dfrac{\overline{\omega}_i}{\overline{\omega}_0}M\right]}{\text{sinc}^2\left(\pi\dfrac{\overline{\omega}_i}{\overline{\omega}_0}\right)}, \tag{D7}$$

implying

$$P = \frac{(q')^2 v}{2\pi\varepsilon_0 D_{\text{int}}}\,\frac{\pi}{2}\sum_i \text{W}_i\,\text{sinc}^2\left(\frac{\alpha}{2}\frac{\overline{\omega}_i}{\overline{\omega}_0}\right)\frac{\text{sinc}^2\left[\pi\dfrac{\overline{\omega}_i}{\overline{\omega}_0}M\right]}{\text{sinc}^2\left(\pi\dfrac{\overline{\omega}_i}{\overline{\omega}_0}\right)}, \tag{D8}$$

α being the length of one microbunch, normalized as a phase relative to the fundamental wavelength. In order to demonstrate Eq. (D7) we assume M microbunches each one of a phase α

$$\begin{aligned}\left\langle\left\langle\cos\left[\frac{\overline{\omega}_i}{\overline{\omega}_0}(\chi_{\mu}-\chi_{\nu})\right]u(\chi_{\mu}-\chi_{\nu})\right\rangle_{\nu}\right\rangle_{\mu} &= \frac{1}{M}\sum_{n=0}^{M-1}\frac{1}{M}\sum_{m=0}^{M-1}\frac{1}{\alpha}\int_{2\pi n-\alpha/2}^{2\pi n+\alpha/2} dx\frac{1}{\alpha}\int_{2\pi n-\alpha/2}^{2\pi n+\alpha/2} dy\,\cos\left[\frac{\overline{\omega}_i}{\overline{\omega}_0}(x-y)\right]u(x-y)\\ &= \frac{1}{M^2}\sum_{\substack{n=0\\ m=0}}^{M-1}\frac{1}{\alpha}\int_{-\alpha/2}^{+\alpha/2} dy\,\cos\left\{\frac{\overline{\omega}_i}{\overline{\omega}_0}[2\pi(n-m)+x-y]\right\}u[2\pi(n-m)+x-y]\\ &= \frac{1}{M^2}\,\text{Re}\left\{\sum_{\substack{n=0\\ m=0}}^{M-1}u(u>m)\,\frac{1}{\alpha}\int_{-\alpha/2}^{\alpha/2} dx\frac{1}{\alpha}\int_{-\alpha/2}^{\alpha/2} dy e^{j(\overline{\omega}_i/\overline{\omega}_0)[2\pi(n-m)+x-y]}\right.\\ &\quad\left.+\sum_{n=0}^{M-1}\frac{1}{\alpha}\int_{-\alpha/2}^{\alpha/2} dx\frac{1}{\alpha}\int_{-\alpha/2}^{\alpha/2} dy e^{j(\overline{\omega}_i/\overline{\omega}_0)(x-y)}u(x-y)\right\}.\end{aligned} \tag{D9}$$

In this last step we took advantage of the fact a charge in one of the microbunches affects all the trailing bunches. The integration over x and y is straightforward leading to

$$\left\langle\left\langle\cos\left[\frac{\overline{\omega}_i}{\overline{\omega}_0}(\chi_{\mu}-\chi_{\nu})\right]u(\chi_{\mu}-\chi_{\nu})\right\rangle_{\nu}\right\rangle_{\mu} = \text{sinc}^2\left(\frac{\alpha}{2}\frac{\overline{\omega}_i}{\overline{\omega}_0}\right)\left\{\frac{1}{M^2}\text{Re}\left[\sum_{\substack{n=0\\ m=0}}^{M-1}u(n>m)e^{j2\pi(\overline{\omega}_i/\overline{\omega}_0)(n-m)}\right]+\frac{1}{2M}\right\}. \tag{D10}$$

The term in the square brackets may be shown (using geometric series) to equal

$$\mathrm{Re}\left[\sum_{\substack{n=0\\m=0}}^{M-1} u(n>m)e^{j2\pi(\bar{\omega}_i/\bar{\omega}_0)(n-m)}\right] = \frac{1}{2}M^2\frac{\mathrm{sinc}^2\left[\pi\dfrac{\bar{\omega}_i}{\bar{\omega}_0}M\right]}{\mathrm{sinc}^2\left(\pi\dfrac{\bar{\omega}_i}{\bar{\omega}_0}\right)} - \frac{1}{2}M \tag{D11}$$

leading to Eq. (D7) and consequently to Eq. (D8).

[1] Y. C. Huang, D. Zheng, W. M. Tulloch, and R. L. Byer, Appl. Phys. Lett. **68**, 753 (1996).
[2] J. D. Lawson, IEEE Trans. Nucl. Sci. **26**, 4217 (1979).
[3] P. M. Woodward, J. IEE **93**, 1554 (1946).
[4] X. E. Lin, Phys. Rev. ST Accel. Beams **4**, 051301 (2001).
[5] P. Yeh and A. Yariv, Opt. Commun. **19**, 427 (1976).
[6] P. Yeh, A. Yariv, and E. Marom, J. Opt. Soc. Am. **68**, 1196 (1978).
[7] Y. Xu, R. K. Lee, and A. Yariv, Opt. Lett. **25**, 1756 (2000).
[8] Y. Xu, G. X. Ouyang, R. K. Lee, and A. Yariv, J. Lightwave Technol. **20**, 428 (2002).
[9] S. G. Johnson, M. Ibanescu, M. Skorobogatiy, O. Weisberg, T. D. Engeness, M. Soljačić, S. A. Jacobs, J. D. Joannopoulos, and Y. Fink, Opt. Express **9**, 748 (2001).
[10] M. Ibanescu, S. G. Johnson, M. Soljačić, J. D. Joannopoulos, Y. Fink, O. Weisberg, T. D. Engeness, S. A. Jacobs, and M. Skorobogatiy, Phys. Rev. E **67**, 046608 (2003).
[11] Y. Fink, D. J. Ripin, S. Fan, C. Chen, J. D. Joannopoulos, and E. L. Thomas, J. Lightwave Technol. **17**, 2039 (1999).
[12] B. Temelkuran, S. D. Hart, G. Benoit, J. D. Joannopoulos, and Y. Fink, Nature (London) **420**, 650 (2002).
[13] T.-B. Zhang, J. L. Hirshfield, T. C. Marshall, and B. Hafizi, Phys. Rev. E **56**, 4647 (1997).
[14] A. Tremaine, J. Rosenzweig, and P. Schoessow, Phys. Rev. E **56**, 7204 (1997).
[15] L. Xiao, W. Gai, and X. Sun, Phys. Rev. E **65**, 016505 (2001).
[16] C. Jing, W. Liu, L. Xiao, W. Gai, P. Schoessow, and T. Wong, Phys. Rev. E **68**, 016502 (2003).
[17] M. Rosing and W. Gai, Phys. Rev. D **42**, 1829 (1990).
[18] K.-Y. Ng, Phys. Rev. D **42**, 1819 (1990).
[19] S. Y. Park and J. L. Hirshfield, Phys. Rev. E **62**, 1266 (2000).
[20] L. Schächter and D. Schieber, Nucl. Instrum. Methods Phys. Res. A **388**, 8 (1997).
[21] L. Schächter, Phys. Rev. E **68**, 036502 (2003).
[22] L. Schächter, *Beam-Wave Interaction in Periodic and Quasi-Periodic Structures* (Springer, Berlin, 1997), p. 199.
[23] C. M. de Sterke, I. M. Bassett, and A. G. Street, J. Appl. Phys. **76**, 680 (1994).
[24] P. Yeh, J. Opt. Soc. Am. **65**, 742 (1979).
[25] B. C. Stuart, M. D. Feit, A. M. Rubenchik, B. W. Shore, and M. D. Perry, Phys. Rev. Lett. **74**, 2248 (1995).
[26] L. Schächter, R. L. Byer, and R. H. Siemann, in *Advanced Acceleration Concepts Workshops*, Mandalay Beach, CA, 2003 (AIP, Melville, NY, 2003), Vol. 647, pp. 310–323.